

AD735744

HL  
HRL 71-0248

AF 61052 - 70 - C - 0005  
FSR - III.

MAY 1971

Technion Research &  
Development Foundation  
Haifa, Israel

**FINAL SCIENTIFIC REPORT - PART III.**

**MEASUREMENTS OF HEAT TRANSFER RATES BEHIND AXIALLY  
SYMMETRIC BACKWARD FACING STEPS IN THE SHOCK TUBE  
AND THE SHOCK TUNNEL**

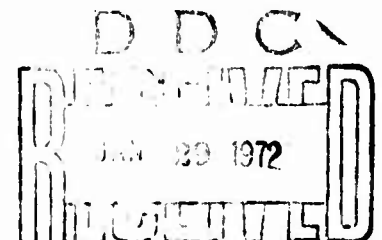
BY

**M. GREEN and J. ROM**

Department of Aeronautical Engineering  
Technion - Israel Institute of Technology,  
Haifa, Israel

**T. A. E. REPORT No. 127**

Reproduced by  
**NATIONAL TECHNICAL  
INFORMATION SERVICE**  
Springfield Va 22151



B

78

DOCUMENT CONTROL DATA - R&D

(Security classification of title, body of abstract and indexing annotation must be entered when the overall report is classified)

1 ORIGINATING ACTIVITY (Corporate author) Technion Research and Development Foundation Aeronautical Engineering Laboratory, Haifa, Israel.		2a REPORT SECURITY CLASSIFICATION UNCLASSIFIED	
		2b GROUP	
3 REPORT TITLE Measurements of Heat Transfer Rates behind Axially Symmetric Backward Facing Steps in the Shock Tube and Shock Tunnel.			
4 DESCRIPTIVE NOTES (Type of report and inclusive dates) FINAL SCIENTIFIC REPORT			
5 AUTHOR(S) (Last name, first name, initial) M. GREEN J. ROM			
6 REPORT DATE MAY 1971		7a TOTAL NO OF PAGES 33	7b NO OF REFS 26
8a CONTRACT OR GRANT NO. F61052-70-C-0005		9a ORIGINATOR'S REPORT NUMBER(S) T.A.E. REPORT No. 127	
b PROJECT NO 7063			
c DoD Element 61102F			
d DoD Subelement 681307		9b OTHER REPORT NO(S) (Any other numbers that may be assigned this report) ARL 71-0268	
10 AVAILABILITY/LIMITATION NOTICES <i>Approved for public release; distribution unlimited</i>			
11 SUPPLEMENTARY NOTES TECH OTHER		12 SPONSORING MILITARY ACTIVITY AEROSPACE RESEARCH LABORATORIES (ARN) WRIGHT-PATTERSON, AFB, OHIO, 45433	
13 ABSTRACT Measurements of heat transfer rates on cone-cylinder models and in the separated regions behind an axially symmetric backward facing step are reported. The measurements were obtained in the shock tube at flow Mach numbers between 1.4 to 2.5, Re/cm of $8 \times 10^3$ to $2 \times 10^5$ and stagnation to wall enthalpy ratios of 10 to 30, and in the shock tunnel at flow Mach number 5.5 and Re/cm of $2.3 \times 10^3$ and $3.6 \times 10^3$ . It is found that the heat transfer in the separated region is practically unaffected by the variation of the flow Mach number from the above supersonic values obtained in the shock tube to the hypersonic value obtained in the shock tunnel. While the unit Reynolds number, Re/cm, is found to be an important parameter in determining the heat transfer rates, particularly the peak values found in the reattachment zones. The position of the maximum heating rate is influenced by the step height and by the forebody length. It is found that the point of maximum heating moves downstream with increasing step height while increasing forebody length causes an upstream movement of this point.			

14 KEY WORDS	LINK A		LINK B		LINK C	
	ROLE	WT	ROLE	WT	ROLE	WT
Heat Transfer Rates						
Axially Symmetric Backward Facing Steps						
Shock tube and Shock Tunnel						

# INSTRUCTIONS

1. **ORIGINATING ACTIVITY:** Enter the name and address of the contractor, subcontractor, grantee, Department of Defense activity or other organization (corporate author) issuing the report.
- 2a. **REPORT SECURITY CLASSIFICATION:** Enter the overall security classification of the report. Indicate whether "Restricted Data" is included. Marking is to be in accordance with appropriate security regulations.
- 2b. **GROUP:** Automatic downgrading is specified in DoD Directive 5200.10 and Armed Forces Industrial Manual. Enter the group number. Also, when applicable, show that optional markings have been used for Group 3 and Group 4 as authorized.
3. **REPORT TITLE:** Enter the complete report title in all capital letters. Titles in all cases should be unclassified. If a meaningful title cannot be selected without classification, show title classification in all capitals in parenthesis immediately following the title.
4. **DESCRIPTIVE NOTES:** If appropriate, enter the type of report, e.g., interim, progress, summary, annual, or final. Give the inclusive dates when a specific reporting period is covered.
5. **AUTHOR(S):** Enter the name(s) of author(s) as shown on or in the report. Enter last name, first name, middle initial. If military, show rank and branch of service. The name of the principal author is an absolute minimum requirement.
6. **REPORT DATE:** Enter the date of the report as day, month, year, or month, year. If more than one date appears on the report, use date of publication.
- 7a. **TOTAL NUMBER OF PAGES:** The total page count should follow normal pagination procedures, i.e., enter the number of pages containing information.
- 7b. **NUMBER OF REFERENCES:** Enter the total number of references cited in the report.
- 8a. **CONTRACT OR GRANT NUMBER:** If appropriate, enter the applicable number of the contract or grant under which the report was written.
- 8b, &c, & 8d. **PROJECT NUMBER:** Enter the appropriate military department identification, such as project number, subproject number, system numbers, task number, etc.
- 9a. **ORIGINATOR'S REPORT NUMBER(S):** Enter the official report number by which the document will be identified and controlled by the originating activity. This number must be unique to this report.
- 9b. **OTHER REPORT NUMBER(S):** If the report has been assigned any other report numbers (either by the originator or by the sponsor), also enter this number(s).
10. **AVAILABILITY/LIMITATION NOTICES:** Enter any limitations on further dissemination of the report, other than those

imposed by security classification, using standard statements such as:

- (1) "Qualified requesters may obtain copies of this report from DDC."
- (2) "Foreign announcement and dissemination of this report by DDC is not authorized."
- (3) "U. S. Government agencies may obtain copies of this report directly from DDC. Other qualified DDC users shall request through \_\_\_\_\_."
- (4) "U. S. military agencies may obtain copies of this report directly from DDC. Other qualified users shall request through \_\_\_\_\_."
- (5) "All distribution of this report is controlled. Qualified DDC users shall request through \_\_\_\_\_."

If the report has been furnished to the Office of Technical Services, Department of Commerce, for sale to the public, indicate this fact and enter the price, if known.

11. **SUPPLEMENTARY NOTES:** Use for additional explanatory notes.

12. **SPONSORING MILITARY ACTIVITY:** Enter the name of the departmental project office or laboratory sponsoring (paying for) the research and development. Include address.

13. **ABSTRACT:** Enter an abstract giving a brief and factual summary of the document indicative of the report, even though it may also appear elsewhere in the body of the technical report. If additional space is required, a continuation sheet shall be attached.

It is highly desirable that the abstract of classified reports be unclassified. Each paragraph of the abstract shall end with an indication of the military security classification of the information in the paragraph, represented as (TS), (S), (C), or (U).

There is no limitation on the length of the abstract. However, the suggested length is from 150 to 225 words.

14. **KEY WORDS:** Key words are technically meaningful terms or short phrases that characterize a report and may be used as index entries for cataloging the report. Key words must be selected so that no security classification is required. Identifiers, such as equipment model designation, trade name, military project code name, geographic location, may be used as key words but will be followed by an indication of technical context. The assignment of links, rules, and weights is optional.

F 61052-70-C-0005

FSR - III

MAY 1971

FINAL SCIENTIFIC REPORT - PART III

MEASUREMENTS OF HEAT TRANSFER RATES BEHIND AXIALLY  
SYMMETRIC BACKWARD FACING STEPS IN THE SHOCK TUBE  
AND THE SHOCK TUNNEL.

by

M. GREEN and J. ROM  
Department of Aeronautical Engineering  
Technion - Israel Institute of Technology,  
HAIFA, ISRAEL.

T.A.E. REPORT 127

This document has been approved for public release and sale; its distribution is unlimited.

The research reported in this paper has been sponsored in part by the Aerospace Research Laboratories, under Contract F61052-70-C-0005, through the European Office of Aerospace Research (OAR) United States Air Force. This research is part of the separated flow research program of the ARL, Thermomechanics Division

### ABSTRACT

Measurements of heat transfer rates on cone-cylinder models and in the separated regions behind an axially symmetric backward facing step are reported. The measurements were obtained in the shock tube at flow Mach numbers between 1.7 to 2.5,  $Re/cm$  of  $8 \times 10^3$  to  $2 \times 10^5$  and stagnation to wall enthalpy ratios of 10 to 30, and in the shock tunnel at flow Mach number 5.5 and  $Re/cm$  of  $2.3 \times 10^3$  and  $3.6 \times 10^3$ . It is found that the heat transfer in the separated region is practically unaffected by the variation of the flow Mach number from the above supersonic values obtained in the shock tube to the hypersonic value obtained in the shock tunnel. While the unit Reynolds number,  $Re/cm$ , is found to be an important parameter in determining the heat transfer rates, particularly the peak values found in the reattachment zones. The position of the maximum heating rate is influenced by the step height and by the forebody length. It is found that the point of maximum heating moves downstream with increasing step height while increasing forebody length causes an upstream movement of this point.

TABLE OF CONTENTS

	<u>PAGE No.</u>
ABSTRACT	I
LIST OF SYMBOLS	III
LIST OF FIGURES	IV - V
1. INTRODUCTION	1 - 4
2. EXPERIMENTAL APPARATUS	5
2.1. The Shock Tube and the Shock Tunnel	5 - 7
2.2. The Vacuum System	7 - 8
2.3. The Measurement System	8 - 13
3. THE MODELS	14 - 16
4. EXPERIMENTAL METHOD	17
4.1. Shock Tube	17 - 18
4.2. Shock Tunnel	18 - 21
5. RESULTS AND DISCUSSION	22
5.1. Zero Step Height Axisymmetric Models - Cone - Cylinder	22 - 23
5.2. Finite Step Height Axisymmetric Models	23 - 25
5.3. Comparison of the Separated Flow Measurements with the Cone-Cylinder (Zero Step Height) Axisymmetric Models and with the Flat Plate Heat Transfer Rates	25 - 28
5.4. Heat Transfer in the Separated Flow Region	29
6. CONCLUSIONS	30
REFERENCES	31 - 33

LIST OF SYMBOLS

$C_p$	specific heat
$h$	step height
$I_o$	thin-film gage constant current
$K$	thermal conductivity
$L$	effective forebody length
$M_f$	flow Mach number
$M_s$	incident shock Mach number
$Nu$	Nusselt number
$Pr$	Prandtl number
$q$	heat transfer rate
$q_{f.p.}$	flat plate heat transfer rate
$q_{s.c.}$	cone-cylinder, zero step height heat transfer rate
$R_o$	thin-film gage initial resistance
$Re$	Reynolds number
$Re_L$	Reynolds number based on effective forebody length
$Re_x$	Reynolds number based on effective length to a point
$t$	time
$\Delta v$	voltage drop across the thin-film gage
$x$	effective distance to a point
$\Delta x$	distance from the separation point
$\alpha$	thermal resistivity
$\rho$	density

LIST OF FIGURES

FIGURE No.

1. Main Parts of the Shock Tube and Shock Tunnel.
2. General View of the Shock Tube and Shock Tunnel.
3. View of the Shock Tunnel.
4. General View of the Electronic Instrumentation.
5. Axisymmetric Separated Flow Model Forebodies.
6. Axisymmetric Model Dimensions.
7. View of the Thin-Film Heat Transfer Gages.
8. Model 11 Configuration and Dimensions.
9. Shock Tube Measurement Port.
10. Shock Tunnel Model Mounting Adapter.
11. Oscilloscope Trace from an Experiment in the Shock Tube.
12. Oscilloscope Trace from an Experiment in the Shock Tunnel.
13. Shock Tunnel Heat Transfer Data.
14.  $Nu_x/Pr$  as a Function of  $Re_x$  for Model 9.
15.  $Nu_x/Pr$  as a Function of  $Re_x$  for Model 10.
16.  $(Nu_x/Pr)/cm$  as a Function of  $\Delta x$  for Model 1.
17.  $(Nu_x/Pr)/cm$  as a Function of  $\Delta x$  for Model 2.
18.  $(Nu_x/Pr)/cm$  as a Function of  $\Delta x$  for Model 3.
19.  $(Nu_x/Pr)/cm$  as a Function of  $\Delta x$  for Model 4.
20.  $(Nu_x/Pr)/cm$  as a Function of  $\Delta x$  for Model 5.
21.  $(Nu_x/Pr)/cm$  as a Function of  $\Delta x$  for Model 6.
22.  $(Nu_x/Pr)/cm$  as a Function of  $\Delta x$  for Model 7.
23.  $(Nu_x/Pr)/cm$  as a Function of  $\Delta x$  for Model 8.

LIST OF FIGURES (CONT'D)

FIGURE No.

24.  $(Nu_x/Pr)/cm$  as a Function of  $Re/cm$  for Model 1.
25.  $[(Nu_x/Pr)/cm]_{max}$  as a Function of  $h$ .
26.  $[(Nu_x/Pr)/cm]_{max}$  as a Function of  $h$ .
27.  $[(Nu_x/Pr)/cm]_{max}$  as a Function of  $Re/cm$
28.  $q/q_{s.c.}$  as a Function of  $\Delta x$  for Model 1.
29.  $q/q_{s.c.}$  as a Function of  $Re/cm$  for Model 1.
30.  $q/q_{f.p.}$  as a Function of  $\Delta x/h$  for Model 3.
31.  $q/q_{f.p.}$  as a Function of  $Re_L$  for Model 3.
32.  $(q/q_{f.p.})_{max}$  as a Function of  $h$ .
33.  $(q/q_{f.p.})_{max}$  as a Function of  $Re_L$ .
34. Maximum Heat Transfer Rate at Reattachment as a function  
of  $(\Delta x/h)_{max}$
35.  $(Nu_x/Pr)/cm$  as a function of  $\Delta x$  for Model 11.

## I. INTRODUCTION

Heat transfer rates to a body in a flowing gas have been studied for many years both experimentally and analytically. In general these studies have concerned themselves with fairly regular geometries such as flat plates, cones, etc. and the theoretical results are well substantiated by experimental results. Heat transfer rates in separated flows, i.e., flow generated by protuberances, steps, sharp edges, etc., lack in general both a well defined theoretical basis and experimental data upon which to establish or substantiate a theory. Interest in separated flows results from the fact that whereas flow separation at subsonic velocity is an unstable phenomena, in the super and hypersonic regime the separated flow is quite stable, remaining laminar even at relatively high Reynolds numbers (similar to the attached flows, Ref. 1). As one might expect, in a separated flow region the heat transfer rates to a surface are lower than those found under comparable attached flow conditions, however, at reattachment the heat transfer rates may be many times higher than those found for the attached flow. Therefore the average heat transfer rate may be higher or lower than that found in attached flow depending upon the "thermal severity" of the reattachment.

The importance of this is immediately obvious. Aircraft and missiles which travel at hypersonic velocities have numerous protuberances of various shapes and sizes, the locally high heating rates resulting from flow reattachment may have damaging effects if not provided for or prevented.

The key of course to solving problems of this type is a knowledge and understanding of the separated flow heat transfer phenomenon.

The heat transfer phenomena occurring in separated flows was first studied by Chapman (Ref. 2) who, by means of a theoretical calculation, compared the heat transfer rates in a separated laminar region with those of a corresponding attached laminar boundary layer. Although the conditions which Chapman investigated were somewhat restrictive, the results of this work showed a marked reduction of the heat transfer rate in the separated region when compared with similar attached flow conditions. Subsequent experimental work (Ref. 3) verified the conclusions arrived at by Chapman, but in addition, as mentioned previously, showed that a marked increase (several times that of the equivalent attached flow heat transfer rate) was experienced upon reattachment of the flow.

A theoretical approach to the problem of heat transfer in the reattachment region of separated boundary layers was later given by Chung and Viegas (Ref. 4) in which the fluid was considered to be flowing normal to the wall at reattachment, such as flow over a cavity. Chung and Viegas compared their theoretically calculated heat transfer rates in the reattachment zone with the experimental results of Larson (Ref. 3) and, although Larson's results were for a separated laminar boundary layer reattaching angle of about  $45^{\circ}$ , the calculation was within 10% of the measured values.

The results of Chapman and of Chung and Viegas are limited by the fact that zero initial boundary layer thickness and uniform external flow is assumed. In addition, these methods determine only average heat transfer rates whereas a knowledge of the local heat transfer rate distribution is of practical importance.

In an attempt to overcome these difficulties, Seginer and Rom [5] used the Crocco-Lees mixing theory modified to include the case of non-adiabatic flows. The results obtained agreed qualitatively with experiments, namely, low heat transfer rates in the separated region and high heat transfer rates in the reattachment region, however, this type of analysis is limited to cases for which the mixing functions and correlation relations are available or may be estimated.

From the preceding discussion it is seen that a theoretical solution to the separated flow heat transfer problem is not available and the theories that presently exist are quite limited in their application providing at best only a qualitative approximation to the problem. It would be expected then that an experimental approach would at least provide guidelines for eliminating the deficiencies in the theory, however, to date this has not been the case. Although many experimental studies have been performed, relatively few local heat transfer rate measurements have been made and, in general, the studies concerned a wide variety of flow models limited to a small numbers of flow conditions. References 6 to 15 present separated flow heat transfer measurements for a number of model geometries and flow

conditions. Systematic comparison of these results is difficult however, in general, regardless of model geometry, peaks in the heat transfer rate were observed in the reattachment region for completely laminar flows and for flows in which transition occurred prior to reattachment, the shorter the distance from the flow separation point to the reattachment point the higher the reattachment heat transfer rates and a dependence of heat transfer rate predominantly on Reynolds number is suggested.

The purpose of the present work is to provide separated flow heat transfer rate data for a wide range of flow conditions and for models, the dimensions of which are systematically varied so as to isolate the effects of the various dimensions on the heat transfer rates. Local heat transfer rates were measured in the "dead water" and reattachment regions by the use of thin platinum film resistance thermometers as described in [16] and the work was performed in a shock tube and a shock tunnel so that the experiments covered a relatively wide range of flow conditions. In the shock tube the range of flow Mach numbers extended from 1.7 to 2.5 and the Reynolds number per centimeter range extended from approximately  $5.0 \times 10^3$  to  $1.5 \times 10^5$ . The work in the shock tunnel provided an ideal means of investigating the dependence of the heat transfer rate on Reynolds number, two values of Reynolds number per centimeter were used,  $2.3 \times 10^3$  and  $3.6 \times 10^3$ , with a flow Mach number of 5.5 for both cases. For the range of Reynolds number experienced in these experiments, laminar flow is expected in all cases with the exception of perhaps the highest Reynolds numbers per centimeter, depending upon the model dimensions.

## 2. EXPERIMENTAL APPARATUS

### 2.1. The Shock Tube and the Shock Tunnel

The shock tube is a device for generating high energy, high velocity gas flow and the shock tunnel is a device by which the high energy gas produced in the shock tube is accelerated to hypersonic velocity. The theory, design and construction of shock tubes and tunnels are described in many previous works (for example, Refs. 17 and 18).

The shock tube and tunnel configuration is schematically shown in Fig.1 and a photograph is shown in Fig. 2. The main parts of the structure are: 1) the high pressure or driver gas section, 2) the diaphragm, 3) the low pressure driven gas section and 4) the supersonic nozzle. A complete description of the shock tube system is presented in [19], however for the sake of completeness a brief outline is provided herein.

The high pressure section is made from a circular steel tube with an internal diameter of 80mm and an external diameter of 115mm and is designed to an internal pressure of 3000 psi. The tube is two meters long and is sealed at one end by a flange through which the driver gas is introduced into the shock tube. The other end of the tube is closed by a copper diaphragm. High pressure commercially available bottled hydrogen was used as the driver gas in all of the experiments.

The diaphragm is located between the driver and driven gas sections and prior to an experiment, separates and maintains the pressure difference between the two sections. The pressure in the driver gas section is controlled by this diaphragm which is designed to burst at a predetermined pressure. For the present work two pressure levels were used, 300 psi and 600 psi and to obtain these

pressures two types of diaphragm were used. The 300 psi diaphragm was made from 0.25mm thick copper sheet and the 600 psi diaphragm from 0.50mm thick copper sheet. Both types of diaphragm were scribed with a cross to a depth of 0.1mm by the use of a lathe cutting tool. The scribing controlled the bursting pressure and provided relatively "clean" bursting of the diaphragm. "Clean" bursting of the diaphragm is desirable so as to minimize disturbances in the initial shock tube flow. Distribution of the bursting pressures around the desired values was  $\pm 5\%$ . The diaphragm is held in place between two flanges by 8 bolts around the circumference of the flanges.

The low pressure section is made from two steel plates and two steel U sections bolted together so as to form a 75 x 75 mm square cross-section, 7 meters long tube. The tube is bolted together with rubber tape and sealant compound between the plates to provide low pressure leak tight joints. Measurement ports are provided in the tube wall along the last three meters of the tube near the supersonic nozzle and 20cm from the same end of the tube are located windows through which models may be installed and/or photographs taken. Near the center of the tube the low pressure pumping system is connected by way of a 2 inch diameter exhaust pipe. The driven gas, which is found in this section of the shock tube, was room temperature air for all of the experiments.

The supersonic nozzle is connected to the end of the driven gas section by way of a convergent section which reduces from the 75 x 75mm cross-section to 15 x 15mm at the throat. Prior to an experiment the shock tube and the supersonic nozzle are separated by a cellophane diaphragm. This diaphragm bursts upon arrival of the incident shock-wave. The supersonic nozzle itself consists

of two divergent sections; the first ends with a fixed area ratio  $A/A^*$ , of 78. The second section is a constant 200mm wide, however the height may be varied, thereby varying the flow properties in the test section. The first section of the nozzle is tilted at an angle of  $10^\circ$  with the horizontal so as not to allow solid particles (diaphragm pieces) entrained in the flow to enter the test section. The entrance to the second section of the nozzle is smaller than the exit of the first section; by this arrangement only the core of the flow is further accelerated by the nozzle thereby minimizing the boundary layer build-up. An external envelope provides a vacuum tight enclosure for the two sections of the nozzle and to this envelope is also connected the nozzle vacuum system piping. Windows are located on both sides of the nozzle at the test section and it is through these windows that models may be installed and/or photographs taken. For these experiments one of the windows was replaced by a blank window made of steel with measurement ports in it; tunnel static pressure was monitored through one of these ports.

An overall view of the shock tube and tunnel is presented in Fig. 2. The high pressure section is shown in the foreground and a diaphragm is shown in place between the high and low pressure sections. A view of the shock tunnel is shown in Fig. 3 with the large dump tank on the left and the entrance to the tunnel on the right.

## 2.2. The Vacuum System

Since different pressure levels are required in the shock tube and the tunnel nozzle, the vacuum system is composed of two systems, one serving the

shock tube and the other serving the shock tunnel nozzle. The system serving the shock tube consists of an Edwards-Kinney KD-110 vacuum pump and is capable of reducing the pressure in the driven gas section to less than 2mm of mercury (absolute). The pressure in this section is regulated by a valve between the pump and the shock tube which controls the amount of air evacuated.

Evacuation of the shock tunnel nozzle was done by three stages of pumps connected in series. A Leybold S-60 rotation vacuum pump to reduce the pressure from atmospheric to several millimeters of mercury, a Leybold Ruvac 25 roots blower type vacuum pump to reduce the pressure to less than 0.25mm Hg and an Edward-Speedvac F-603 diffusion pump which reduced the pressure to its final value of approximately 20 $\mu$  Hg.

### 2.3. The Measurement System

Pressure Measurements were made by the use of piezoelectric pressure transducers for static pressure measurements during the experiments in the shock tunnel. Details of these transducers are given in Table 1. Kistler Model 504 charge amplifiers were used to convert the pressure transducer output charge to a pressure dependent voltage. Pressure measurements made prior to the experiments in the driven gas section, in the driver gas section and in the shock tunnel were made with the gages described in Table 2.

Heat Transfer Rate Measurements were made by the use of thin film platinum resistance thermometers which were made by sputtering a thin film of platinum metal on a pyrex glass backing material. The resistance of the gages varies linearly with temperature so that by passing a small current (20 ma) through the gage and measuring the change in voltage across the gage during an experiment

the temperature variations in the gage may be determined. One of the outstanding characteristics of this gage is its extremely short response time which is less than one microsecond; this property makes it most suitable for work in the shock tube where total experiment times may be on the order of  $50\mu$  seconds. A detailed description of these gages and their calibration is given in Ref. 20.

The output signal from the thin film gages described above is a parabolic function of time for a step function change in the heat transfer rate. This signal may be converted back into a step function which is proportional to the heat transfer rate by the use of an analog network built for this purpose. Such analog networks were built in the Electronics Shop of the Aeronautical Engineering Laboratory and used for the experiments performed in the straight section of the shock tube. Because of the large signal attenuation through the analog networks, low noise differential amplifiers with an amplification of approximately 100 were built and used so as to provide sufficient output signal strength for recording. A complete description of the analog networks may be found in Ref. 21. Calibration details of the thin film gages and the thin film gage - analog network combination is also provided in Ref. 20 briefly, however, calibration consists of exposing the gage to a known heat flux and comparing this with the gage or the analog network output to determine the value of  $(\rho C_p K)_b^{0.5}/\alpha$  in the following expression:

$$q = \left(\pi/2\right) \left(1/I_o R_o\right) (\rho C_p K)_b^{0.5}/\alpha \Delta\sqrt{t}.$$

Heat transfer rates may then be calculated using this relationship since the values of  $(\rho C_p K)_b^{0.5}/\alpha$ ,  $I_o$  and  $R_o$  are known and  $\Delta\sqrt{t}$  is measured in the experiment.

TABLE 1 - PIEZOELECTRIC PRESSURE TRANSDUCERS USED FOR STATIC PRESSURE MEASUREMENTS DURING EXPERIMENTS  
IN THE SHOCK TUNNEL

Location	Model No	Typical Pressure Measure- ment psi	Range of Transducer psi	Elec Output pcb/psi	Response Time $\mu$ sec	Natural Frequency cps	Dimensions inches
End of Shock Tube	601	300	10-3000	1.2	3	130,000	0.25 x 0.60
Shock Tunnel Test Section	606	0.05	0-30	4.4	3	130,000	0.5 x 1.25

TABLE 2 - PRESSURE GAGES FOR MEASUREMENTS PRIOR TO EXPERIMENTS

Location	Pressure Gage	Typical Measurements	Range of Pressure Gage
High Pressure Driver Gas Section	Ashcroft Beryllium Tube Duragauge	300 - 600 psi	0 - 1500 psi
Low Pressure Driven Gas Section	Wallace & Tiernan Model No. Fa 160	2 - 100 mm Hg	0 - 20 mm Hg
	Edwards High Vacuum, Type CG3		0 - 40 mm Hg
	Edwards High Vacuum, Type CG3		0 - 100 mm Hg
Shock Tunnel	Hastings Vacuum Gage - GV - 5	20 $\mu$ Hg	1 - 1000 $\mu$ Hg

For the work in the shock tunnel the output signal from the thin film gages was too small to allow the use of the analog networks for data reduction and it was necessary to reduce the raw data using the method described in Ref. 22 by which the complete heat transfer rate history for the total experiment time is calculated.

Wave Speed Measurements were also made with the help of the same thin film gages described previously. Two pairs of these gages were installed in the four measurement ports in the straight section of the shock tube nearest the supersonic nozzle. The distance between the gages in each pair was known so that by measuring the time taken for the incident shock wave to travel the distance between the gages in each pair, the average wave speed may be calculated for those sections of the shock tube. The thin film gages of course measure only temperature change, however, since the incident shock wave raises the temperature of the gas over which it passes, the gages respond to this temperature change. Each gage pair was connected to one of two counters, either a Beckman Model 7360 or a Model 6146, through a pulse amplifier - current supply module which provided a voltage signal to the counters. This module also supplied the current necessary to produce the initial voltage across the gage. The function of one gage in each pair was to start its respective counter and the other stopped the counter. The resolution of these counters is  $1.0\mu$  seconds and  $0.1\mu$  sec. respectively so that the accuracy of the wave speed measurement was better than  $\pm 1.0\%$ . The signal from one of the thin film wave velocity gages was also used to trigger the recording oscilloscopes.

The Recording System consisted of four Tetronix Oscilloscopes: one model 535, one model 555 and two models 565 oscilloscopes. Output signals from the thin film temperature gages and/or the pressure transducers were fed to the oscilloscopes and the resulting trace photographed on Polaroid film.

A general view of the electronic instrumentation is presented in Fig.

4.

### 3. THE MODELS

A series of 10 axisymmetric models (Fig. 5 ) were used in this work. The configuration and dimensions of the models are given in Fig. 6. Construction of the model is such that the forebodies (the cone-cylinder) are interchangeable. So that the same instrumented pyrex glass cylindrical part on which the platinum films are located is used for all the experiments and only the cone-cylinder forebody is changed to obtain various step heights and forebody lengths. A photograph of the instrumented pyrex cylinder with a mounted forebody is shown in Fig. 7, the 10 thin-film gages are clearly seen here as strips across the cylinder. The platinum film gages are described in Section 2.3 and the gage positions behind the step are given in Table 3. In addition to two forebodies which gave zero step height, four step heights were used: 0.85 mm, 1.90mm, 2.90mm and 4.00mm and two lengths: 10.0mm and 25.0mm, for the cylindrical section of the forebody. The half angle of the forebody cone was  $15^{\circ}$  for all the models. Therefore, the effective forebody length varied with step height. Table 4 presents the effective forebody lengths for each of the 10 models.

In addition to the 10 models already described, a model was fabricated for the purpose of examining the heat transfer rates in the dead water region. This model, designated Model 11, is shown in Fig. 8 and the configuration and dimensions are given in Fig. 8. The model step height is equal to the instrumented cylinder diameter 10.2mm, and the cylindrical forebody length is 25.0mm. As an integral part of the model, a cylindrical section is provided at the model base, the effect of this is to increase the distance of each gage from the separation point by 15.0mm.

TABLE 3 - GAUGE POSITIONS ON THE MODEL

Gauge No.	1	2	3	4	5	6	7	8	9	10
Dist. from Step (mm)	0.69	2.49	4.45	6.36	8.32	10.10	11.97	14.02	16.06	18.03

TABLE 4 - EFFECTIVE CONE-CYLINDER FOREBODY LENGTH FOR THE VARIOUS MODELS

Model	1	2	3	4	5	6	7	8	9	10
Effective Forebody Length L, (mm)	21.50	23.55	25.50	27.60	36.50	38.55	40.50	42.60	19.85	34.85

Mounting of the models in the shock tube was accomplished through the measurement port at the end of the shock tube which is shown in Fig.9. In the shock tunnel the model was mounted, with the aid of the adapter shown in Fig.10, on a perpendicular mounting bar located at the end of the shock tunnel test section. In both the shock tube and the shock tunnel the model axis was aligned with the longitudinal axis of the local section.

#### 4. EXPERIMENTAL METHOD

##### 4.1. Shock Tube

The quantity which determines the flow properties in the shock tube for a given gas combination (hydrogen/air for this work) and a given temperature ratio between these gases (room temperature in all of these cases) is the pressure ratio between the driver and driven gases. For the work performed in the shock tube straight section, the pressure in the driver gas section was 300 psi, so that by varying the pressure in the driven gas section the flow properties are controlled. The range of pressure in this section was from 2mm Hg abs to 100mm Hg absolute, giving a range of incident shock wave Mach numbers from approximately 9.0 to 4.0 and actual flow Mach numbers of 2.5 to 1.7. The actual incident shock Mach number is a measured quantity and knowing this the remaining flow quantities may be determined from the flow charts for equilibrium air found in Ref. 23. It is obvious from these charts that to obtain higher Mach numbers, the initial pressure in the driver gas section,  $p_1$ , must be reduced and the resulting Reynolds number flow parameter,  $Re$ , therefore decreases.

Prior to each experiment the resistance of each gage was measured with a bridge network and the current to each gage was set at 20 ma. Immediately after completion of an experiment the resistance of each gage was again checked and the average value used in reducing the heat transfer rate data.

For the work in the straight section of the shock tube the analog networks described in Section 2.3 were used to convert the thin film gage output into a step function, the height of which is proportional to the heat transfer rate. Reduction of this data was accomplished by measuring, with the aid of a comparator, the height of the output signal as recorded by the oscilloscope. Since this output signal is directly proportional to the heat transfer rate, it is a relatively simple matter, knowing the calibration coefficient of a given gage-analog network combination, to calculate the heat transfer rate. The comparator used has a resolution of 0.001mm. Fig. 11 is an example of the data recorded during a shock tube experiment, the upper trace is that of the thin-film gage parabolic output signal, the lower trace is the signal obtained after processing by an analog network. In practice, the lower trace is measured at several places and the average reading is then used.

#### 4.2. Shock Tunnel

The work in the shock tunnel was of a slightly different nature, since the flow Mach number is determined by the nozzle area ratio. For the present work the nozzle was fixed in a position which gave a Mach number of 5.5 as determined by the shock tunnel calibration described in Ref. 19. The shock tunnel was operated at the tailored interface condition (also described in Ref. 19) so as to obtain maximum test time. By this method, the shock tube is operated at conditions which give an undisturbed high pressure, high temperature standing air reservoir at the end of the shock tube. Table 5 presents the typical shock tube conditions for the operation of the tailored

shock tunnel. This air is then accelerated by the nozzle to the desired flow Mach number according to the nozzle area ratio setting. By controlling the pressure in this standing air reservoir (the pressure in the reservoir is the stagnation pressure of the nozzle flow) the Reynolds number in the nozzle is varied, the flow Mach number however, remains unchanged. Two Reynolds numbers were used, as previously mentioned, the higher of the two was obtained using the shock tube as described in Section 2.1 and to obtain the lower one a convergent-divergent nozzle was installed between the high pressure, driver gas section and the copper diaphragm. The flow conditions thereby obtained in the shock tunnel are shown in Table 6. A complete description of the shock tunnel and its calibration may be found in Ref 19.

The data reduction procedure for the shock tunnel work was somewhat different than that used for the shock tube. The maximum output voltage from the thin film gages for the shock tunnel work was less than 3 millivolts. This output voltage level was less than that required to obtain a useful output from the amplifier analog network combination. In addition, the shock tunnel output signal shown in Fig. 12 is substantially different than that obtained in the shock tube (Fig. 11). In Fig. 11 the voltage signal from a thin film gage prior to processing by the analog network shows an almost immediately parabolic response after passage of the incident shock wave so that, as described in Ref. 20, a step function change in the heat transfer rate occurs and steady flow conditions are achieved almost immediately. In contrast to this, the starting process in the shock tunnel is substantially slower (Ref. 24) and steady flow conditions, as illustrated by the parabolic

TABLE 5 - SHOCK TUBE CONDITIONS FOR OPERATION OF THE TAILORED INTERFACE SHOCK TUNNEL

Ms	P mm Hg	T <sub>1</sub> °K	H Btu/lb	T <sub>0</sub> °K	Z	γ	$\mu$ $\frac{\text{kg sec}}{\text{m}^2}$	P ata		$\rho$ $\frac{\text{kg sec}^2}{\text{m}^4}$	
6	35	300	2100	3500	1.03	1.21	$8.4 \times 10^{-6}$	14.8 with nozzle	23.5	0.15 with nozzle	0.22

TABLE 6 - AVERAGE TEST SECTION FLOW PROPERTIES

Mach Number	P ata (mm Hg)	Po <sub>2</sub> ata	T °K	U m/sec	Re/m l/m
5.5.	$6.8 \times 10^3$ (5)	0.33	550	2850	$3.6 \times 10^5$ * $2.3 \times 10^5$

\* with nozzle in the high pressure section.

portion of the output signal in Fig. 12 are not achieved until some 2.5 milliseconds after the tunnel starts to operate (the time required for tunnel starting depends upon the ratio between the initial pressure in the tunnel and the initial pressure in the driven gas section). In order to convert this output signal to a heat transfer rate it was necessary to measure, with the aid of the comparator, the magnitude of the output signal as a function of time and by a numerical integration employing the trapezoidal rule of the data reduction equation appearing in Ref. 22, the heat transfer rate was calculated at 100  $\mu$  second intervals from the initiation of flow in the shock tunnel. The results of this calculation were plotted as heat transfer rate versus real test time as in Fig. 13 and the value of the constant heat transfer rate determined. This procedure was carried out for each gage and for each experiment.

## 5. RESULTS AND DISCUSSION

### 5.1. Zero Step Height Axisymmetric Models - Cone - Cylinder.

In order to determine a basis of comparison for the type of axisymmetric models used in the present work, a series of experiments were performed using a model without a backward facing step, a simple cone-cylinder. The dimensions of the two models used in this part of the work designated Models 9 and 10 were presented in Fig. 6. The two forebody lengths were used to check the effect of forebody length on the heat transfer rate and the results of these experiments are presented in Figures 14 and 15 in the form of  $Nu_x/Pr$  vs  $Re_x$  for models 9 and 10, respectively. The results are plotted for each gage and, with the exception of gage number 1 which is located immediately behind the forebody-gage base attachment point, the results are well represented by the correlating relation:

$$Nu_x/Pr = 0.0013 Re_x^{1.0}$$

This relation applies to both models 9 and 10 indicating that for the range of model dimensions tested, the effect of the length upon the relationship between heat transfer rate and flow conditions follows this relation. For the purpose of comparison the line representing the flat plate heat transfer rates for the equivalent flow conditions is also shown in Figs 14 and 15. It is with these results that the data for Models 1 through 8 will be compared.

Despite the fact that the cone-cylinder is a shape which appears frequently in aerodynamic work, no data was found to corroborate the above correlation which exhibits a linear dependence with longitudinal position i.e., the local Reynolds number to the first power, whereas for the case of a flat plate the correlation

contains the local Reynolds numbers to the one-half power.

## 5.2. Finite Step Height Axisymmetric Models

Presented in Figs. 16 to 23 is the quantity  $(Nu_x/Pr)/cm$  which was measured at each gage position (distance behind the separation point) for each of the 8 axisymmetric finite step models (Models 1 through 8 and described in Fig. 6). The quantity  $(Nu_x/Pr)/cm$  is, of course, a heat transfer rate related quantity. The heat transfer rate data is plotted in the figures as a function of gage position using the Reynolds number per centimeter ( $Re/cm$ ) as a parameter. The lower two values of  $Re/cm$ , i.e.  $2.5 \times 10^3$  and  $4 \times 10^3$ , are data from the shock tunnel experiments, the remaining curves are from experiments performed in the shock tube. In all cases, the value of the heat transfer rate increases with increasing  $Re/cm$  for a given gage position. Also, as found in previous investigations, initially low values of  $(Nu_x/Pr)/cm$  are found in the dead water region immediately behind the flow separation point with a subsequent rise and leveling off in the reattachment region. Movement of the reattachment region, which is taken as the region in which the maximum value of  $(Nu_x/Pr)/cm$  is attained, may also be observed. The reattachment region moves upstream toward the separation point with increasing values of  $Re/cm$  and with increasing forebody length and the movement is downstream with increasing step height. Also listed on the Figs. 16 to 23 are the respective values of  $h/L Re_L^{1/2}$ ,  $Re_L$ ,  $M_s$  and  $M_f$  which correspond to each of the curves plotted ( $h/L Re_L^{1/2}$  is a boundary layer thickness related parameter used in Refs. 7, 25 and 26 for correlation of the test data).

In Fig. 24 the heat transfer rate parameter,  $(Nu_x/Pr)/cm$ , for Model 1 is plotted as functions of  $Re/cm$  for each of the 10 gages. This figure is representative of the data of all of the models tested and also illustrates the presence of low heat transfer rates in the dead water region and higher rates in the reattachment region. It is interesting to note the rate of variation of the heat transfer rate for each gage or position behind the separation point. In the dead water region the heat transfer rate rises slowly at the lower values of  $Re/cm$  and rapidly at the higher values of  $Re/cm$ , beyond reattachment the opposite trend is observed. This results in a "concave" variation in the dead water region and a "convex" variation in the reattachment region. The region in which the curve shape changes, that is, where an approximately linear variation is observed, marks the position between the gages which are in the "unattached" and those that are in the "reattached" flows. For Model 1 this occurred at gage 3 or approximately 4.45mm from the separation point. It should be mentioned that this is not the point at which the maximum heat transfer rate occurs but does indicate the region in which the  $Re$  dependence of the heat transfer changes. Also indicated on Fig. 24 is the range of  $Re/cm$  which applies to the shock tube and that which applies to the shock tunnel. It is worth noting that for the shock tunnel experiments the flow Mach number was 5.5 in all cases and the  $Re/cm$  parameter was controlled by varying the supersonic nozzle air stagnation pressure. This may justify the conclusion that the heat transfer rate is predominately a function of Reynolds number and is not dependent on the flow Mach number.

As previously mentioned, knowledge of the value of the maximum heat transfer rate is of importance and for the purpose of illustrating the variation of this parameter with the experimental variables, Figs. 25, 26 and 27 present plots of  $[(Nu_x/Pr)/cm]_{\max}$  as a function of step height with  $Re_L$  as a parameter,  $[(Nu_x/Pr)/cm]_{\max}$  as a function of step height with  $Re/cm$  as a parameter and as a function of  $Re/cm$ , respectively. Several observations may be made from these figures. When plotted using  $Re_L$  as a parameter, the short forebody models experienced heat transfer rates which are higher than those experienced by the long forebody models. When plotted using  $Re/cm$  as a parameter however, the maximum heat transfer rates appear little affected by step height or forebody length for the range of step heights and forebody lengths tested. The predominant affect is that of Reynolds number per centimeter (Fig. 27) i.e., the value of  $[(Nu_x/Pr)/cm]_{\max}$  increases with increasing  $Re/cm$ . This parameter,  $Re/cm$ , is a function of flow conditions independent of model geometry. Also plotted in Fig. 26 is the line which represents the case of zero step height (models 9 and 10) thereby illustrating that for all except the lowest value of  $Re/cm$ ,  $2.5 \times 10^3$ , the maximum value of the separated flow reattachment heat transfer rate is higher than for the equivalent nonseparated flow case.

### 5.3. Comparison of the Separated Flow Measurements with the Cone-Cylinder (Zero Step Height) Axisymmetric Models and with the Flat Plate Heat Transfer Rates

Fig. 28 presents the variation of the measured heat transfer rate for Model 1 related to the cone-cylinder (step height = 0.0) data,  $q/q_{s.c.}$ , as a function of distance from the flow separation point with  $Re/cm$  as a parameter. This figure is representative of the data obtained from the other Models, 2 through 8, which similarly exhibiting values of  $q/q_{s.c.}$  which are low immediately following flow separation and in the dead water region and rise to values of approximately

0.7 to 2.5 in the reattachment zone. Of interest here is the fact that in the dead water region the values of  $q/q_{s.c.}$  decrease to a minimum with increasing  $Re/cm$  and subsequently rise with a further increase in  $Re/cm$ . In the reattachment region, however, the values of  $q/q_{s.c.}$  rises to a maximum with increasing  $Re/cm$  and subsequently decreases with a further increase in  $Re/cm$ . This fact is further illustrated in Fig. 29 which presents  $q/q_{s.c.}$  plotted as a function of  $Re/cm$  for each gage of Model 1, similar curves were obtained for Model 2 through 8. This result is of course consistent with the previously noted trend of a concave heat transfer rate variation in the dead water region and a convex variation beyond the reattachment region.

Reference 25, which presented only the portion of this work that was performed in the shock tube, i.e.  $Re/cm$  from  $5.0 \times 10^3$  to  $1.5 \times 10^5$  compared the heat transfer rate data with the rates expected under similar flow conditions for a flat plate. In Figs. 30 and 31 the results of Ref. 25 have been extended to include the measurements made in the shock tunnel and are representative of the results obtained for each of the 8 models. The figures present  $q/q_{f.p.}$  plotted as a function of  $\Delta x/h$  and as a function of  $Re_L$ , respectively. The dependence of the heat transfer rate ratio,  $q/q_{f.p.}$  on the Reynolds number is evident in these figures. Figs. 32 and 33 have also been extended to include the shock tunnel data and present  $(q/q_{f.p.})_{max}$  as a function of step height for several values of  $Re_L$  and  $(q/q_{f.p.})_{max}$  as a function of  $h/L$ , respectively. It was pointed out in Ref. 25 that the data from the short forebody models (1, 2, 3 and 4) could not be correlated with the data from the long

forebody models (5, 6, 7 and 8) when  $Re_L$  was used as a parameter. In Fig. 26, however, it was seen that when  $[(Nu_x/Pr)/cm]_{max}$  is examined as a function of  $Re/cm$ , the differences due to forebody length and step height changes are reduced considerably, thereby indicating a dependence of the maximum heat transfer rate on flow conditions rather than on model geometry. Movement of the reattachment region however, is affected by model geometry as well as flow conditions. Although a definitive relation among flow parameters, model geometry and reattachment region location was not derived, a trend is apparent as was discussed previously.

The question naturally arises at this point as to which comparison is preferable: i.e. comparison with the expected flat plate values or with the measured data for the cone-cylinder (zero-step height) axisymmetric models. Inasmuch as the correlation obtained for Models 9 and 10 in this work is substantially different than the equivalent correlation for a flat plate, the resulting values of  $(q/q_{f.p.})_{max}$  and  $(q/q_{s.c.})_{max}$  are also different. The maximum value of  $(q/q_{f.p.})_{max}$  for the range of test conditions being 4.0 and for the equivalent  $(q/q_{s.c.})_{max}$ , 2.5. In addition, the maximum value of  $(q/q_{f.p.})_{max}$  occurs at the highest  $Re_L$  whereas  $(q/q_{s.c.})_{max}$  reaches a maximum with increasing  $Re/cm$  and with further increases in  $Re/cm$ , the value decreases. This qualitative difference is due to the exaggeration effect of the steeper slope of the zero step height correlation. The preference here is for the  $(q/q_{s.c.})$  comparison, since it gives a more realistic measure of the reattachment overheating for the case of axisymmetric separated flow.

It would be worthwhile now to review some of the previously published work in the light of the present data. To do this systematically is, however, difficult due to the wide range of model geometries and test conditions used in previous

investigations and the lack of an established theoretical criterion. A trend noticed in previous studies (Ref. 6 to 15) is that higher heat transfer rate peaks are obtained with decreasing reattachment distance,  $\Delta x$ . This, however, appears to be due to the choice of the characteristic length for determining the Reynolds number parameter since in the present work, when based on the  $Re/cm$  parameter, the peak or maximum value is relatively unaffected by step height and forebody length. That this is a characteristic of axisymmetric flow seems unlikely and it is more likely that this indicates the need for a correlation parameter which takes into account reattachment distance and flow conditions and flow properties.

An additional type of comparison is that made in Ref. 26. In Ref. 26 a correlation was formulated which related the maximum heat transfer rate at reattachment with the position of this maximum, independent of model geometry. This correlation is of the form:

$$(q/q_{f.p.})_{\max} = 12 \left(\frac{\Delta x}{h}\right)_{\max}^{-1}$$

where  $\left(\frac{\Delta x}{h}\right)_{\max}$  is the point at which  $(q/q_{f.p.})_{\max}$  first occurs, and was obtained by the compilation of the results of a large number of measurements of heat transfer rates in the reattachment region of various types of models and flow conditions. Data points from the present study, which are compared with this correlation in Fig. 34, seem to be in good agreement with this correlation.

#### 5.4. Heat Transfer in the Separated Flow Region

Model 11 was designed to provide a relatively long separated flow or dead water region. All of the heat transfer gages were expected to be located in the dead water region and accordingly, low heat transfer rates recorded. The model was too large to be tested in the shock tube and therefore only the flow conditions provided by the shock tunnel were used. The data are plotted in Fig. 35 and as mentioned previously, low heat transfer rates were measured. Most of the data is for the higher  $Re/cm$  flow condition ( $3.6 \times 10^3$ ) with only two points plotted at the  $Re/cm$  value of  $2.3 \times 10^3$ . The reason for the lack of data at the lower Reynolds number per centimeter is the low output signal at this flow condition which results in a noise dominated output signal that is difficult to measure. The data that was obtained however, does indicate relatively constant low heat transfer rates with low heat transfer rates occurring at the lower value of  $Re/cm$ . In addition, the rapid heat transfer rate rise which is usually associated with flow reattachment is not seen. The difficulty here, however, is that the expected reattachment heat transfer rates at this value of  $Re/cm$  are also quite low (see Fig. 23) and there may be some difficulty in identifying reattachment. Further discussion in the case of this model is not possible, however, without more complete data.

## 6. CONCLUSIONS

Based upon the experimental results obtained in this investigation several conclusions may be drawn with respect to axisymmetric backward facing step separated flow: (1) maximum heat transfer rates are primarily affected by flow conditions as measured by the  $Re/cm$  parameter; (2) movement of the location of  $[(Nu_x/Pr)/cm]_{max}$  is influenced by step height and by forebody length (when measured by the distance from the separation point,  $\Delta x$ , this point moves downstream with increasing step height and upstream with increasing forebody length); (3) the variation of heat transfer rate with Reynolds number in the separated flow region is different than that in the attached flow region (concave to convex variation) indicating a possible means of defining the thermal reattachment region rather than taking the point of  $[(Nu_x/Pr)/cm]_{max}$  as the "point" of reattachment; and (4) the heat transfer rate is a function of Reynolds number, Mach number having no noticeable affect on the heat transfer rate. The experimental results obtained for the case of zero step height on non-separated flow give a correlation of the form

$$Nu_x = 0.0013 Pr Re_x^{1.0}$$

In Ref. 25 a need was expressed for a new similarity correlation, the present work indicates that a separated flow maximum heat transfer rate correlation may be expected to be a function of the flow properties as expressed by the quantity  $Re/cm$  whereas reattachment location is expected to be a function of the separation geometry.

#### REFERENCES

1. Chapman, D.R., Kuehn, D.M. and Larson, H.K., "Preliminary Report on a Study of Separated Flows in Supersonic and Subsonic Streams", NACA RM A55L14, 1956
2. Chapman, D.R., "A Theoretical Analysis of Heat Transfer in Regions of Separated Flow", NACA TN 3792, 1956.
3. Larson, H.K., "Heat Transfer in Separated Flows", Institute of Aeronautical Sciences, Jan. 1959.
4. Chung, P.H. and Viegas, J.R., "Heat Transfer at the Reattachment Zone of Separated Laminar Boundary Layers", NASA TN D-1072, Sept. 1961.
5. Seginer, A. and Rom, J., "An Integral Method for the Calculation of Heat Transfer Rate in Laminar Supersonic Separated Flows", Israel Journal of Technology, Vol. 6, No. 1-2, (1968), 72-83
6. Rom, J. and Seginer, A., "Laminar Heat Transfer to a Two-Dimensional Backward Facing Step from the High Enthalpy Supersonic Flow in the Shock Tube", AIAA Journal, Vol. 2, No. 2, Feb. 1964, 251-255.
7. Rom, J. and Seginer, A., "Heat Transfer in the Laminar Supersonic Separated Flow Behind an Axially Symmetric Backward Facing Step", Technion - Aeronautical Engineering Dept. TAE Report No. 82, Jan. 1968
8. Rom, J. and Seginer, A., "Laminar and Transitional Heat Transfer in the Two-Dimensional Separated Flow Behind a Sharp Protruding Leading Edge", Technion-Aeronautical Engineering Dept. TAE Report No. 71, Aug. 1967
9. Rom, J. and Seginer, A., "Laminar Heat Transfer to a Two-Dimensional Blunt Base from the High Enthalpy Flow in the Shock Tube", Israel Journal of Technology, Vol. 5, No. 4, (1967), 90-98.

10. Rom, J. and Seginer, A., " Laminar Heat Transfer to a Two-Dimensional Blunt Flat Nosed Body in Transonic and Supersonic Flow", Technion Aeronautical Engineering Dept., TAE Report No. 75, Sept. 1967.
11. Baker, D.J. and Martin, B.W., "Heat Transfer in Supersonic Separated Flow Over a Two-Dimensional Backward Facing Step", International Journal of Heat and Mass Transfer, Vol. 9 (1965), 1081-1088.
12. Naysmith, A. "Measurements of Heat Transfer in Bubbles of Separated Flow in Supersonic Air Streams", ASME and Institute of Mechanical Engineering, London, International Heat Transfer Conference, Part II, 43, 378, 1961.
13. Thomann, L., "Measurements of Heat Transfer and Recovery Temperature in a Separated flow in a Mach Number of 1.8 ", FFA Rept. 82, The Aeronautical Research Inst. of Sweden, Stockholm, Sweden, 1959.
14. Holden, M.S., " Leading Edge Bluntness and Boundary Layer Displacement effects on attached and separated laminar boundary layers in a compression corner", AIAA 6th Aerospace Science Meeting, Paper No. 68-68, Jan. 1968.
15. Sanford, J. and Ginoux, J.J., "Laminar, Transitional and Turbulent Heat Transfer Behind a Backward Facing Step in Supersonic Flow", Technical Note 38, Von Karman Institute for Fluid Dynamics, Rhode-Saint Genese, Belgium, Oct. 1968.
16. Rabinowicz, J., Jessey, M.E. and Barch, C.A., " Resistance Thermometer for Heat Transfer Measurement in a Shock Tube", GALCIT Hypersonic Research Project Memorandum No. 33, July 1956.
17. Glass, I.I. and Hall, J., " Handbook of Supersonic Aerodynamics", Section 18 - Shock Tubes, NAVROD Rep. 1488.

18. Rabinowicz J., "Aerodynamic Studies in the Shock Tube", GALCIT Hypersonic Research Project Memorandum No. 38, June 1957.
19. Kuritzky, A., and Rom, J., "Calibration of the Tailored Interface 8" x 10" Shock Tunnel", Technion - Aeronautical Engineering Dept. TAE REPORT No. 116, Feb. 1971.
20. Seginer, A., Cohen, A., Rom, J., "Calibration of Thin Film Resistance Thermometers for Heat Flux Measurements in the Shock Tube", Israel Journal of Tech., Vol. 3, No. 1, (1965), 25-30.
21. Skinner, G.T., " Analog Network to Convert Surface Temperature to Heat Flux", ARS Journal, Vol. No. 30, June 1960, 569-570.
22. Vidal, R.J., "Model Instrumentation Techniques for Heat Transfer and Force Measurements in a Hypersonic Shock Tunnel, Cornell Aeronautical Laboratory", Inc. Report No. AD-917-A-1, Feb. 1956.
23. Glass, I.I., "Shock Tubes - Part I: Theory and Performance of Simple Shock Tubes", Univ. of Toronto, Institute of Aerophysics, UTIA Review No. 12, Part I, May 1958.
24. Glick, H.S., Hertzberg, A. and Smith, W., " Flow Phenomena in Starting a Hypersonic Shock Tunnel", Cornell Aeronautical Laboratory, Inc., Report No. AD-789-A-3, AEDC-TN-55-16.
25. Green, M. and Rom, J., "Measurements of Heat Transfer Rates Behind Axially Symmetric Backward Facing Steps in the Shock Tube", Technion - Israel Institute of Technology, TAE Report No. 115, Dec. 1970.
26. Rom, J., Seginer, A. and Green, M., " Investigation of Heat Transfer in Base Type Supersonic Laminar and Transitional Separated Flows", Technion - Israel Institute of Technology, TAE Report No. 111, April 1970.

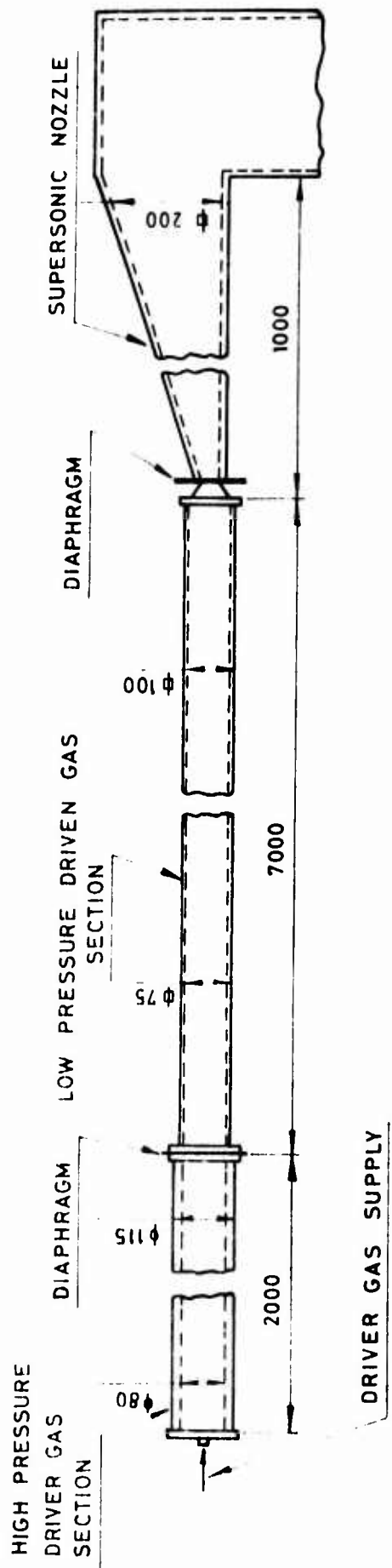


FIGURE 1 - MAIN PARTS OF THE SHOCK TUBE AND SHOCK TUNNEL

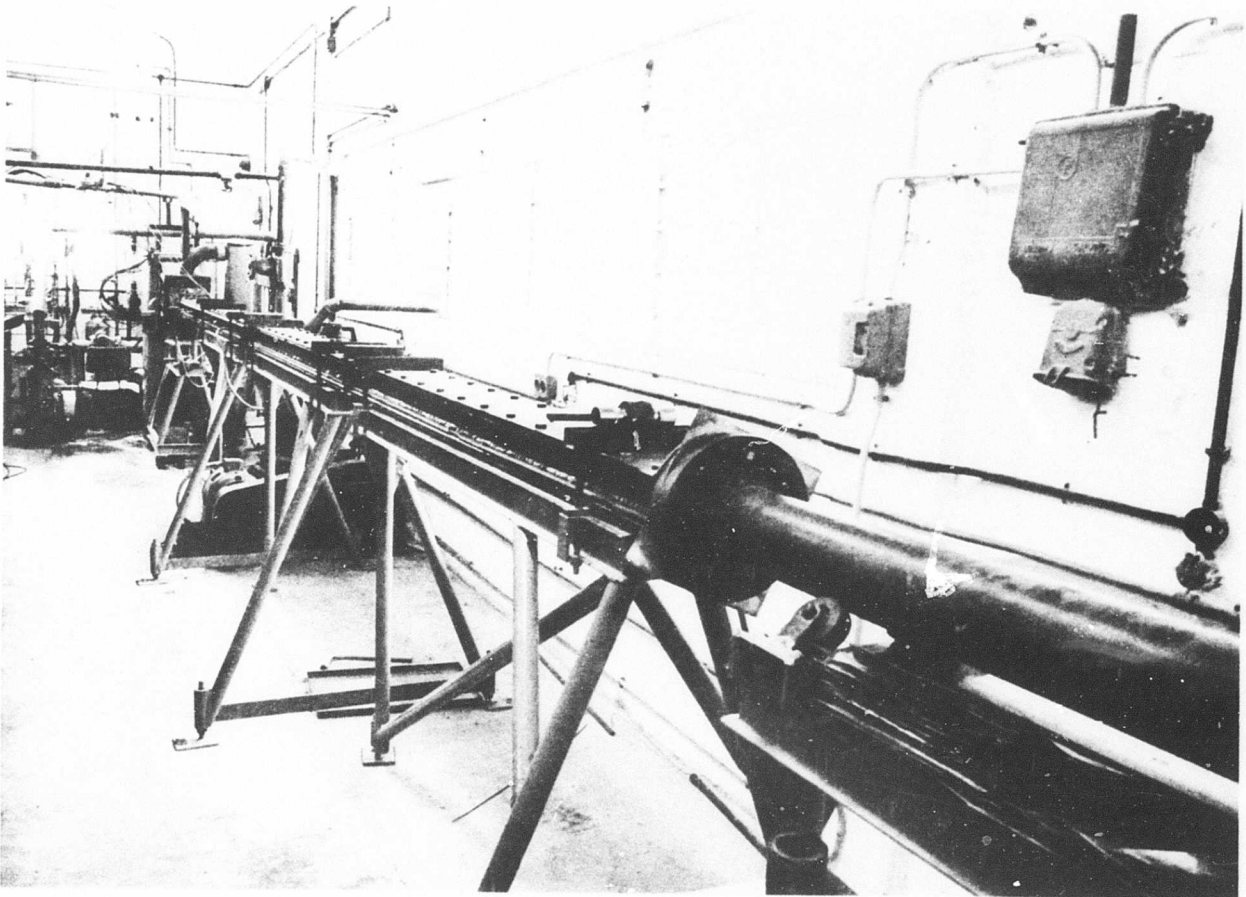


FIGURE 2 - GENERAL VIEW OF THE SHOCK TUBE AND SHOCK TUNNEL

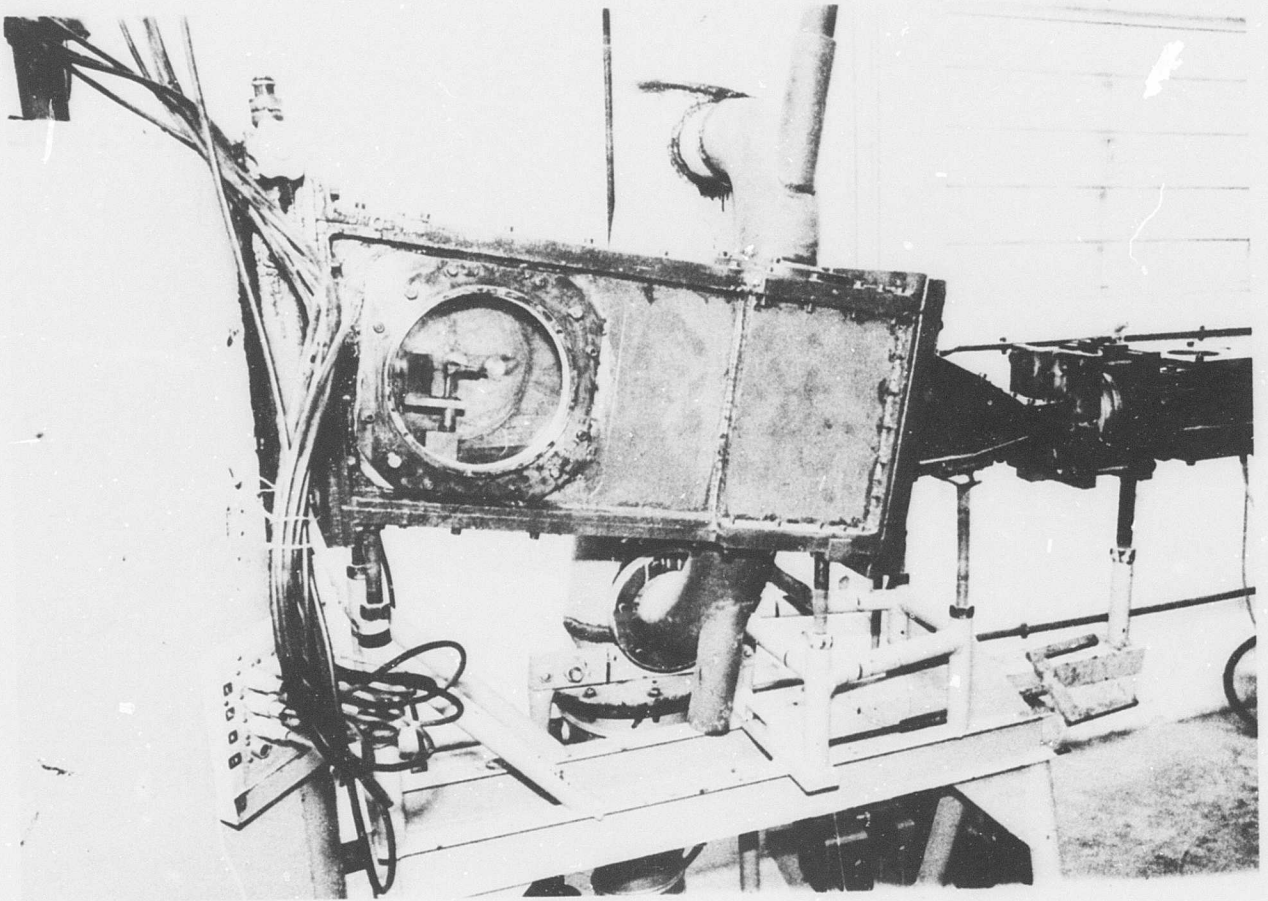


FIGURE 3 - VIEW OF THE SHOCK TUNNEL

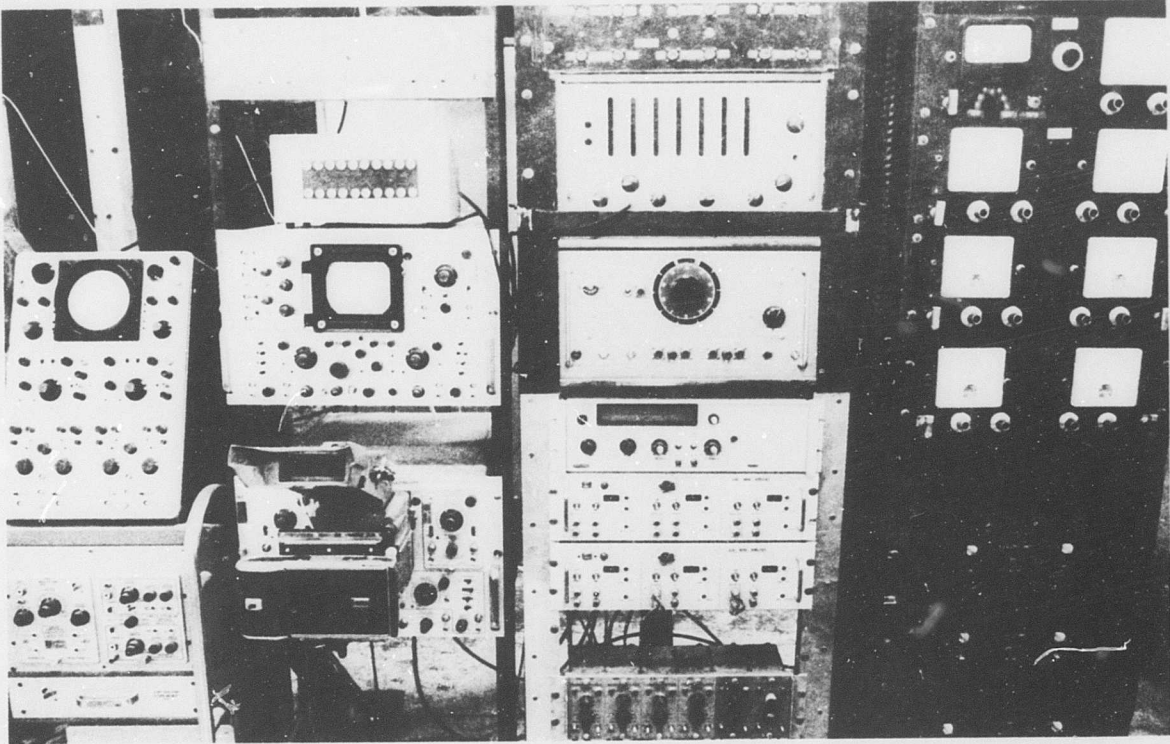


FIGURE 4 - GENERAL VIEW OF THE ELECTRONIC INSTRUMENTATION

L

-38-

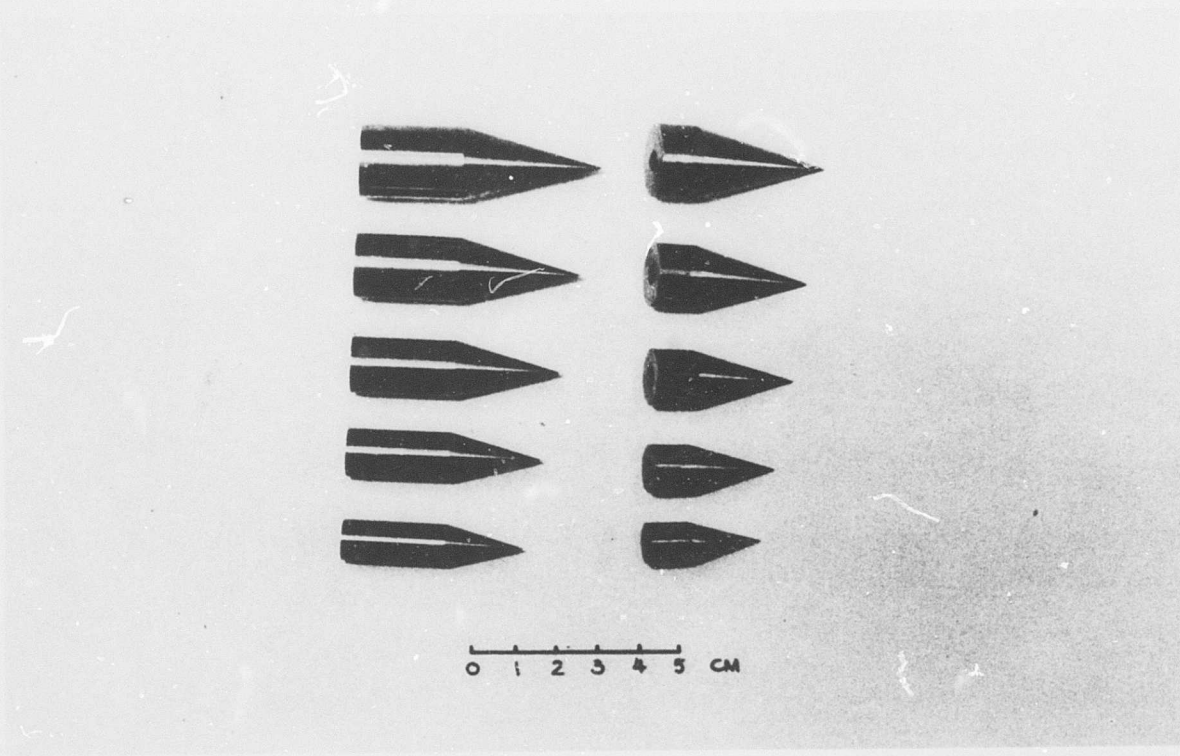
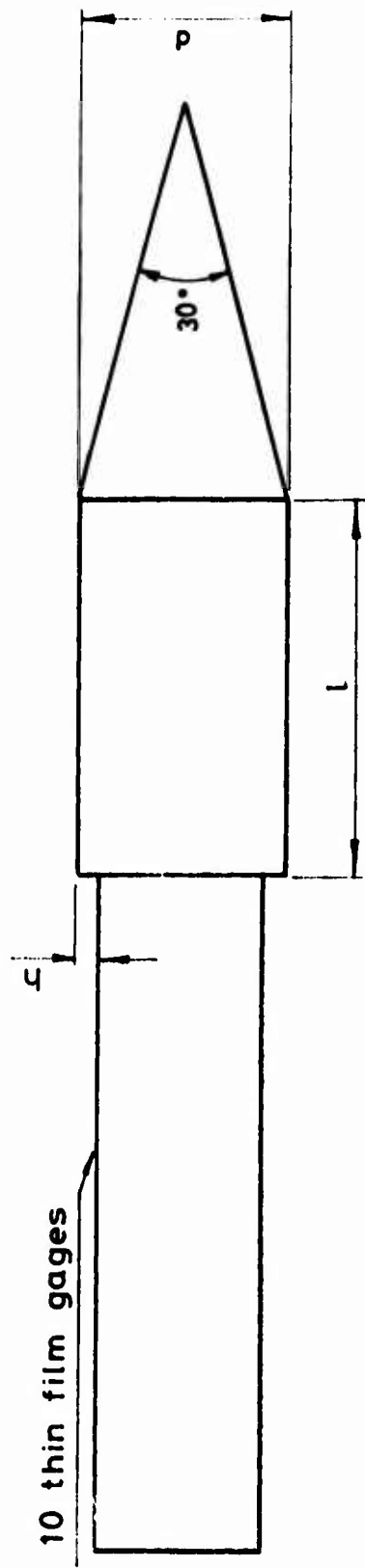


FIGURE 5 - AXISYMMETRIC SEPARATED FLOW MODEL FOREBODIES



MODEL NUMBER	h (mm)	d (mm)	l (mm)
1	0.85	11.90	10.00
2	1.90	14.00	10.00
3	2.90	16.00	10.00
4	4.00	18.20	10.00
5	0.85	11.90	25.00
6	1.90	14.00	25.00
7	2.90	16.20	25.00
8	4.00	18.20	25.00
9	0.00	10.20	10.00
10	0.00	10.20	25.00

FIGURE 6 - AXISYMMETRIC MODEL DIMENSIONS

-40-

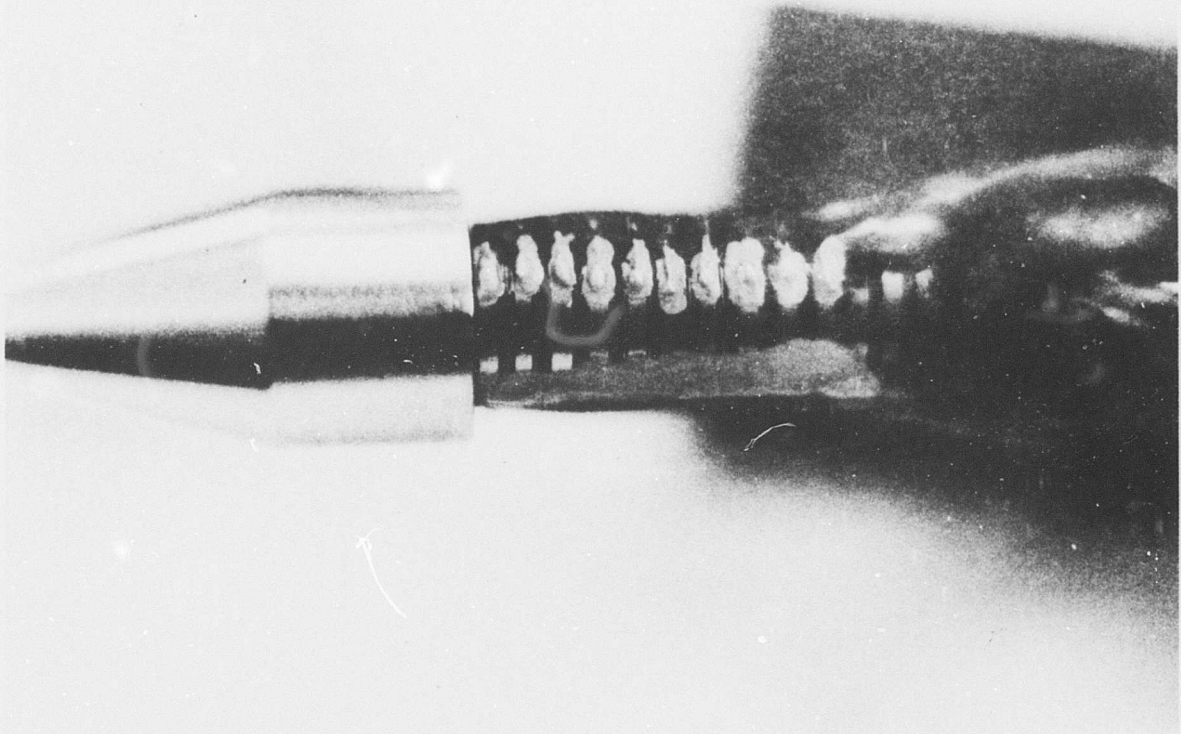
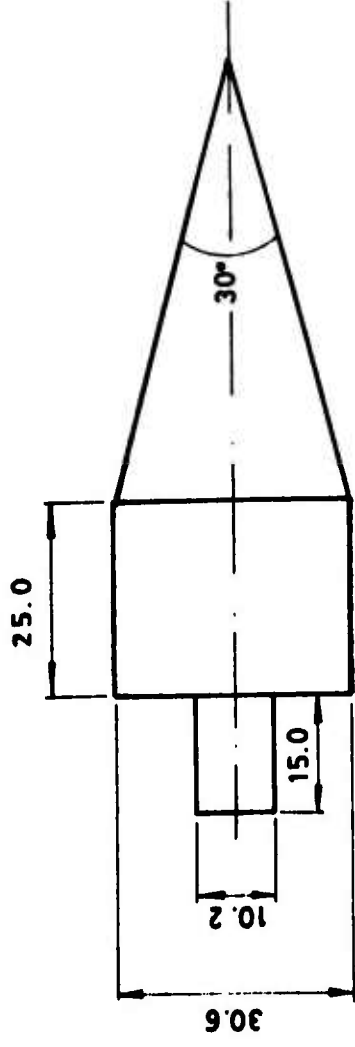


FIGURE 7 - VIEW OF THE THIN-FILM HEAT TRANSFER GAGES



## ALL DIMENSIONS IN MILLIMETERS

FIGURE 8 - MODEL 11 CONFIGURATION AND DIMENSIONS

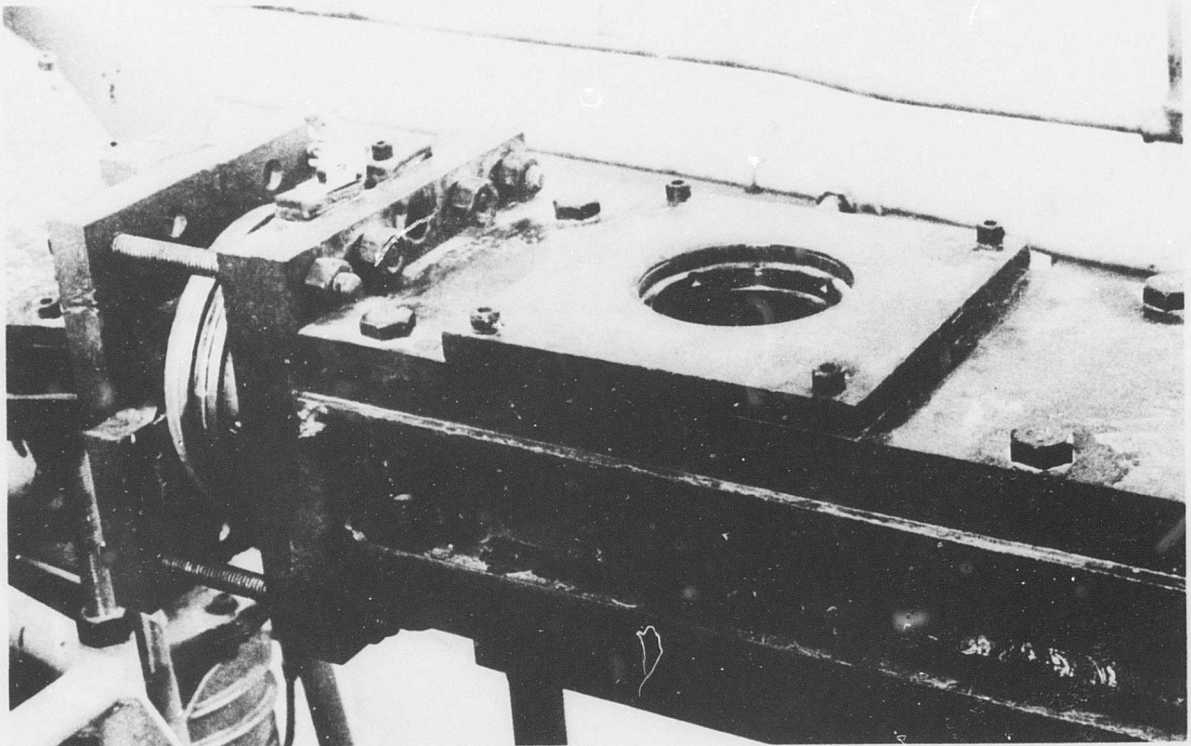


FIGURE 9 - SHOCK TUBE MEASUREMENT PORT

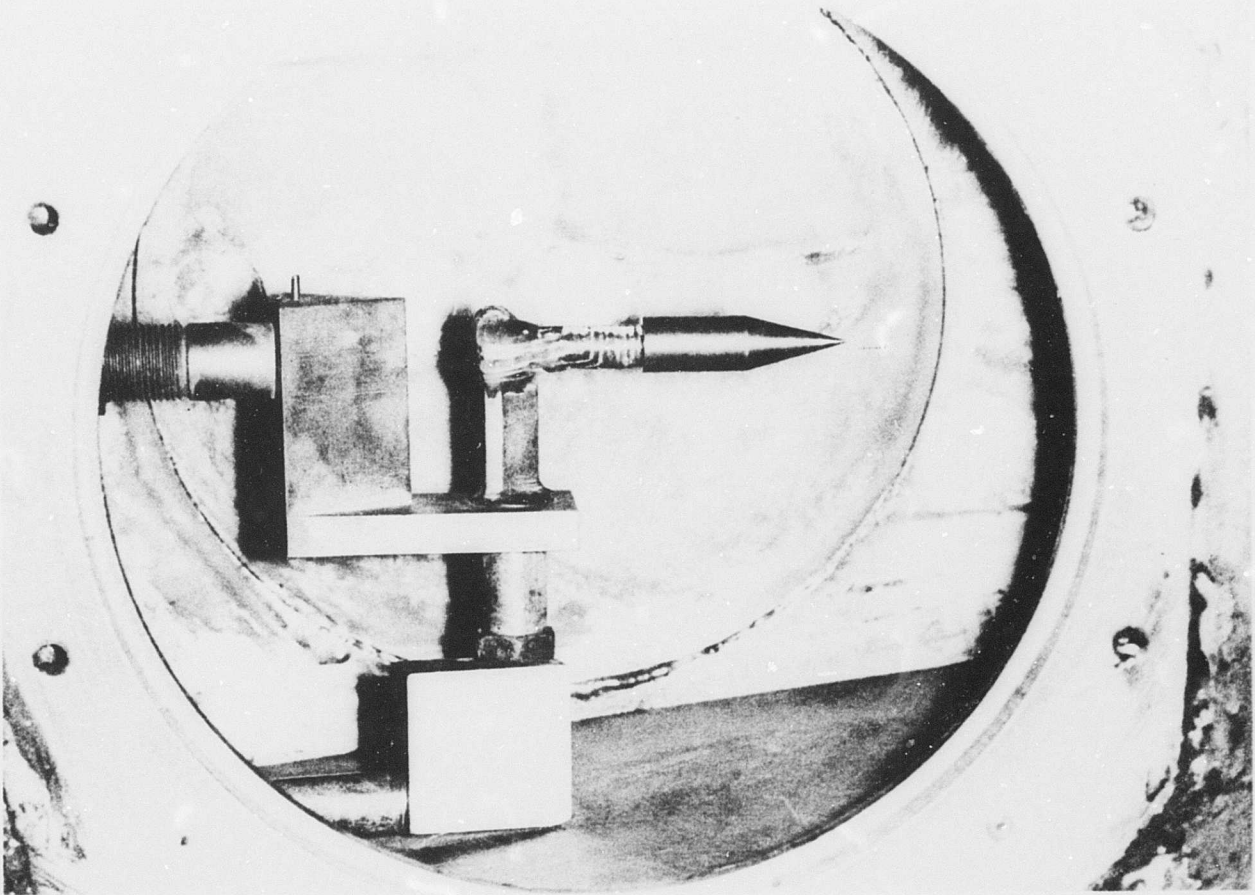
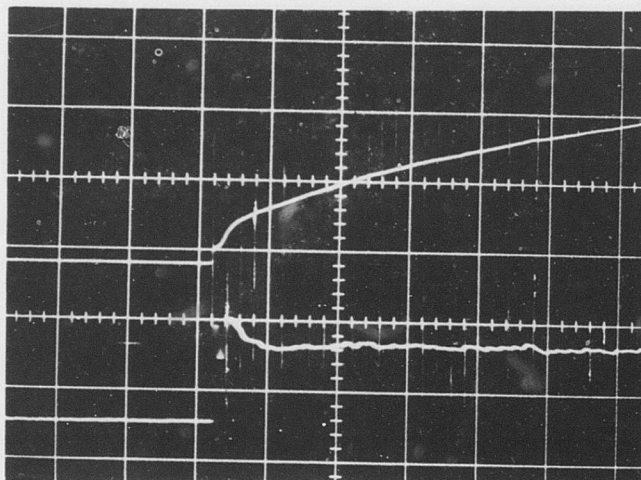


FIGURE 10 - SHOCK TUNNEL MODEL MOUNTING ADAPTER

-44-



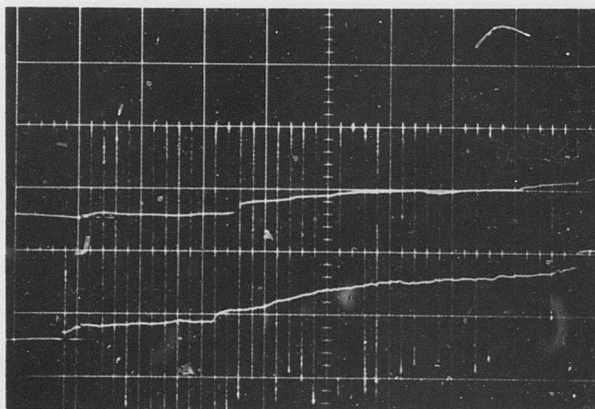
TIME BASE:  $50\mu\text{SEC}/\text{CM}$

AMPLIFICATION:

PARABOLA:  $10\text{mv}/\text{cm}$

STEP:  $100\text{mv}/\text{cm}$

FIGURE 11 - OSCILLOSCOPE TRACE FROM AN EXPERIMENT IN THE SHOCK TUBE



TIME BASE:  $500\mu\text{SEC}/\text{CM}$

AMPLIFICATION:  $1\text{mv}/\text{cm}$

FIGURE 12 - OSCILLOSCOPE TRACE FROM AN EXPERIMENT IN THE SHOCK TUNNEL

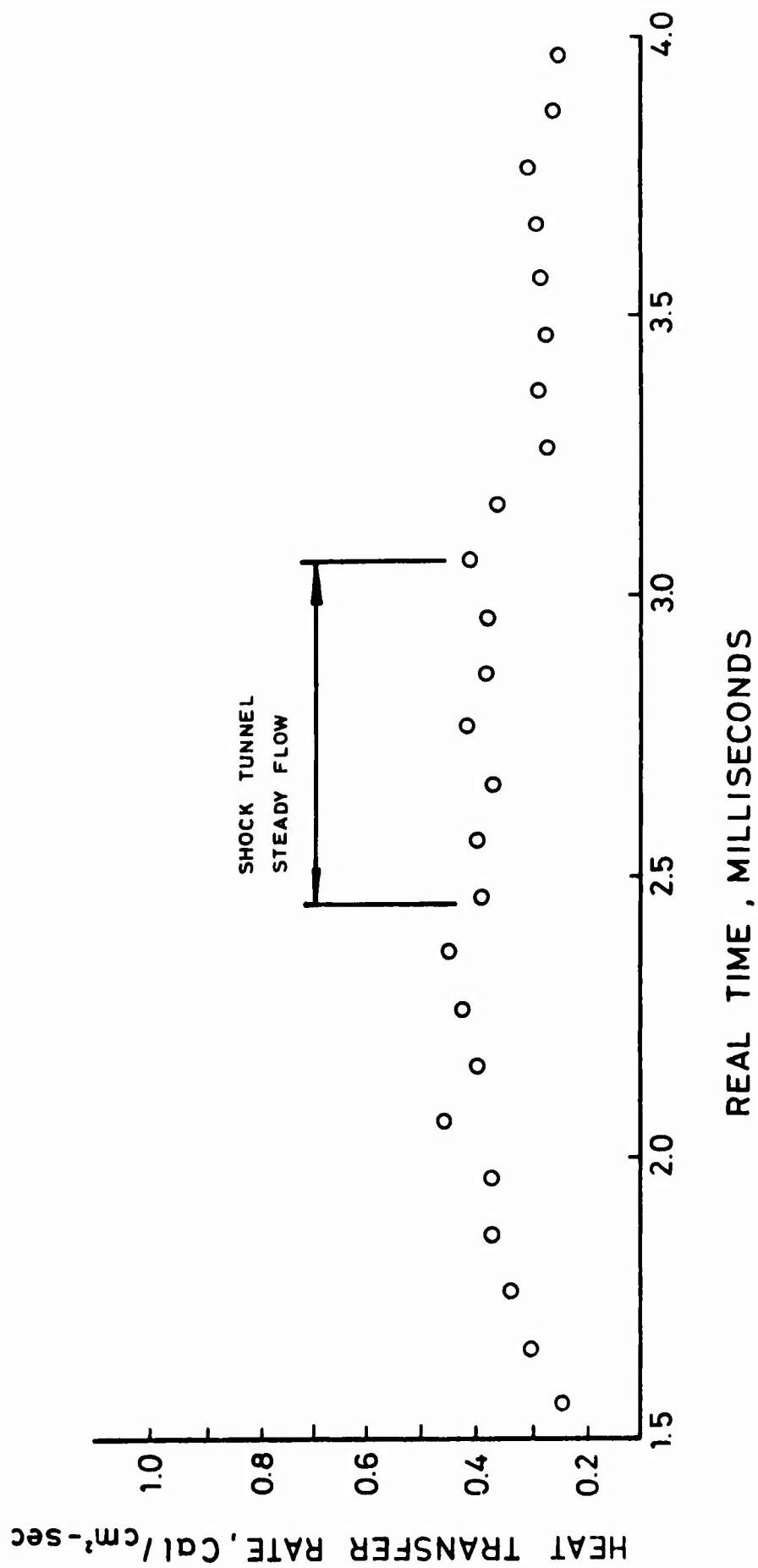


FIGURE 13 - SHOCK TUNNEL HEAT TRANSFER DATA

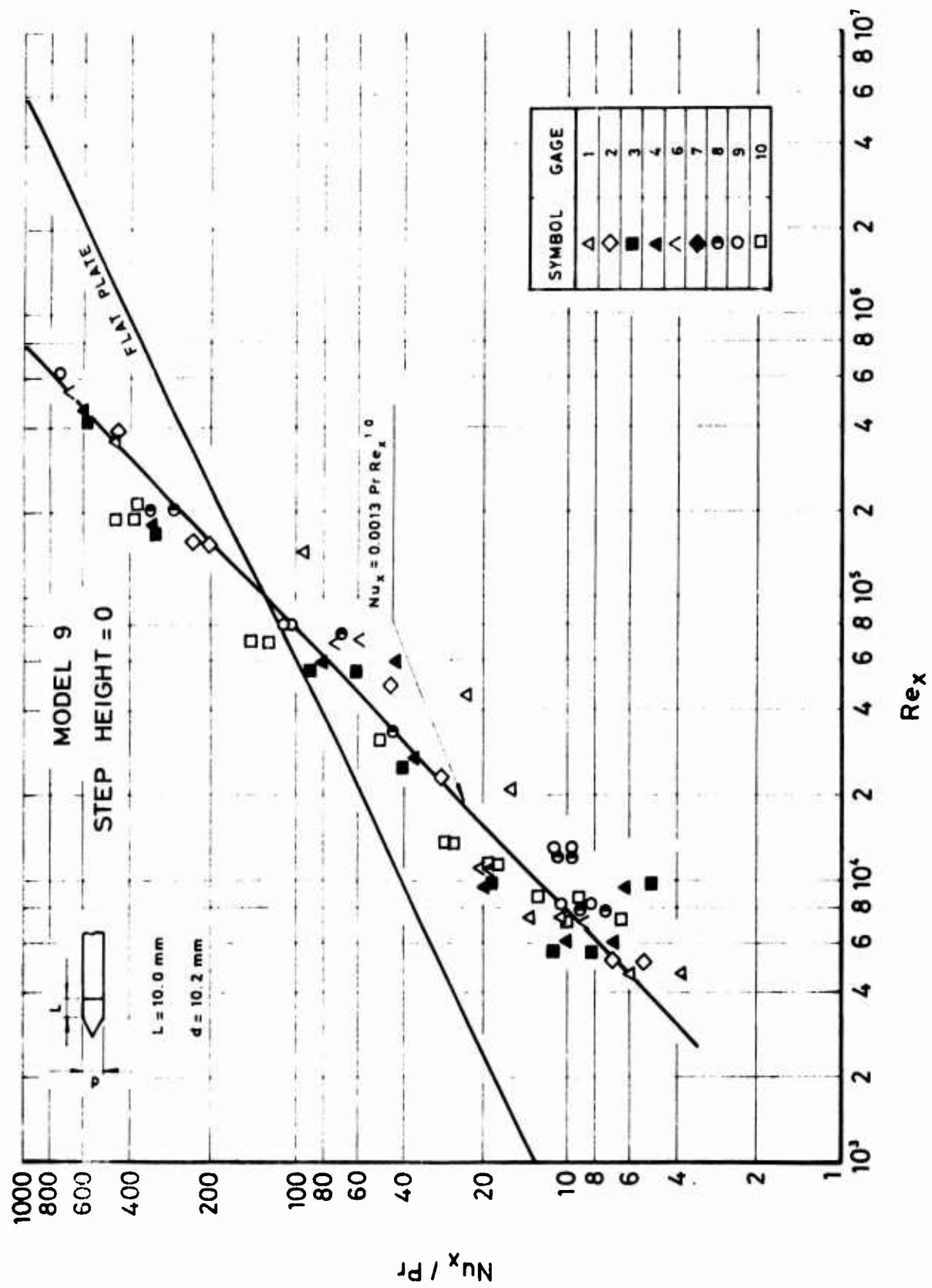


FIGURE 14 -  $Nu_x / Pr$  AS A FUNCTION OF  $Re_x$  FOR MODEL 9

MODEL 10  
STEP HEIGHT=0

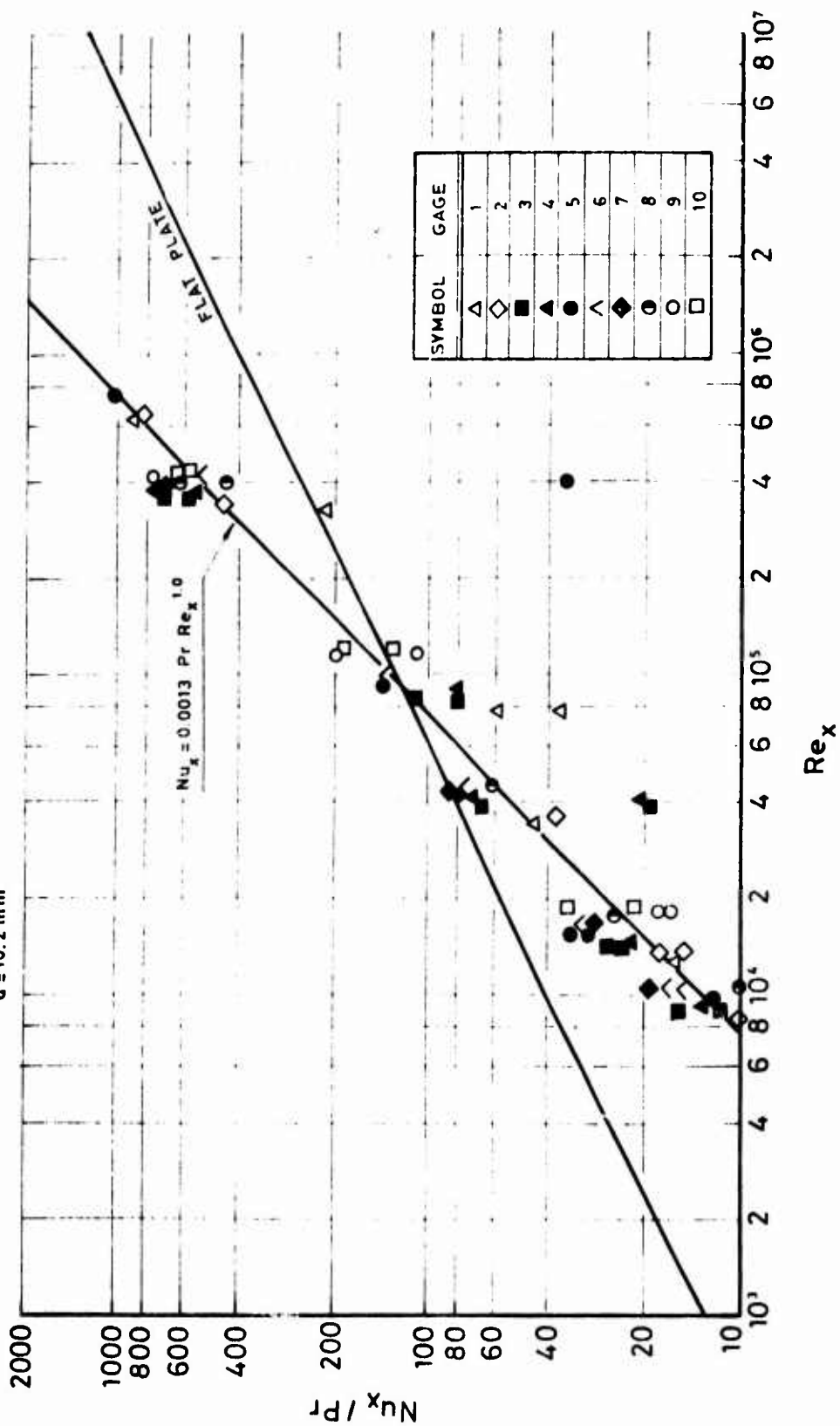


FIGURE 15 -  $Nu_x / Pr$  AS A FUNCTION OF  $Re_x$  FOR MODEL 10

47

MODEL 1  
 $h = 0.85 \text{ mm}$

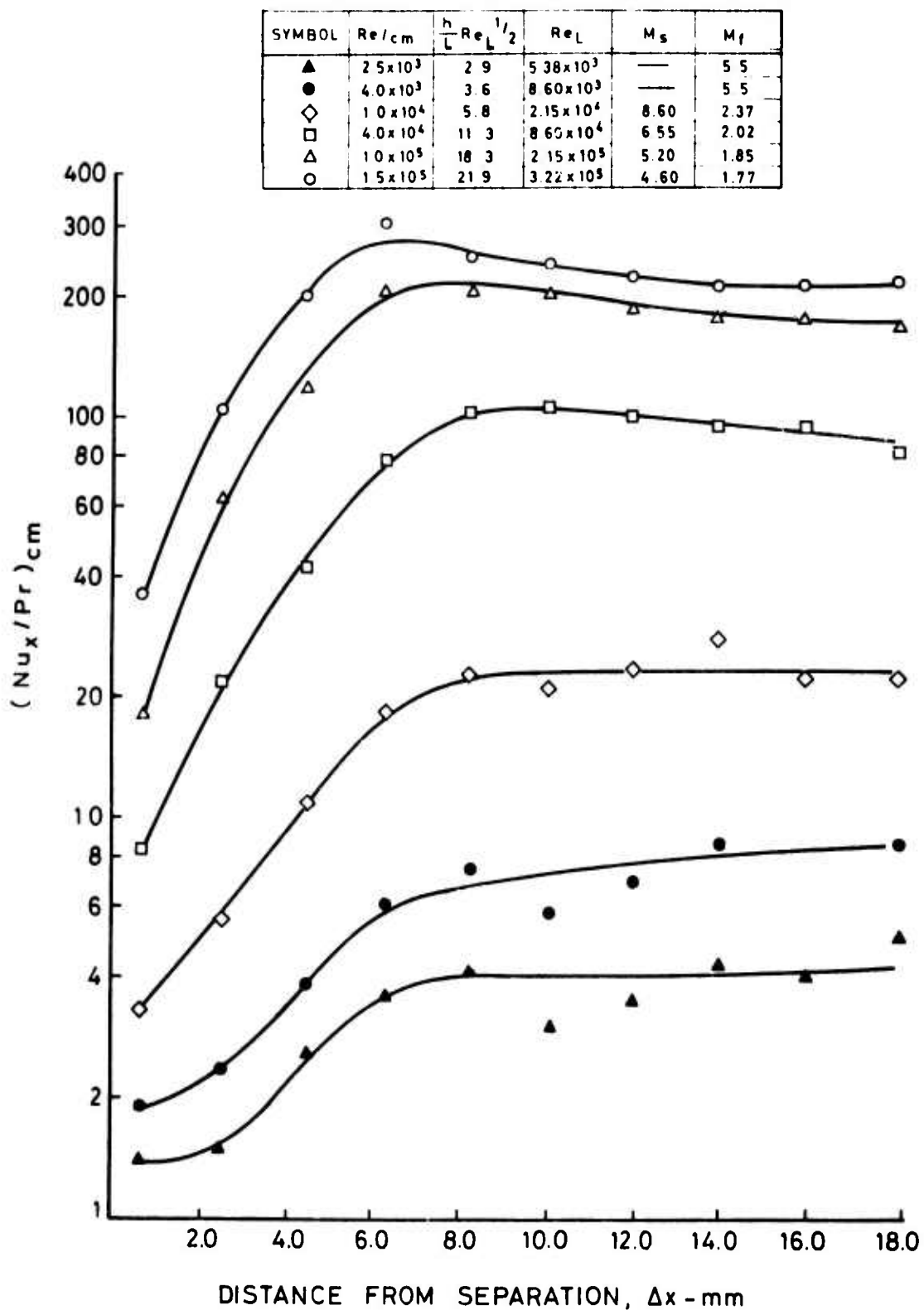


FIGURE 16 -  $(Nu_x/Pr)_{cm}$  AS A FUNCTION OF  $\Delta x$  FOR MODEL 1

MODEL 2  
h=190 mm

SYMBOL	Re/cm	$\frac{h}{L} Re_L^{1/2}$	Re <sub>L</sub>	M <sub>s</sub>	M <sub>f</sub>
▲	$2.5 \times 10^3$	6.2	$5.89 \times 10^3$	—	5.5
●	$4.0 \times 10^3$	7.8	$9.41 \times 10^3$	—	5.5
◇	$1.0 \times 10^4$	12.4	$2.36 \times 10^4$	8.60	2.37
□	$4.0 \times 10^4$	24.7	$9.41 \times 10^4$	6.55	2.02
△	$1.0 \times 10^5$	39.2	$2.36 \times 10^5$	5.20	1.85
○	$1.5 \times 10^5$	47.9	$3.53 \times 10^5$	4.60	1.77

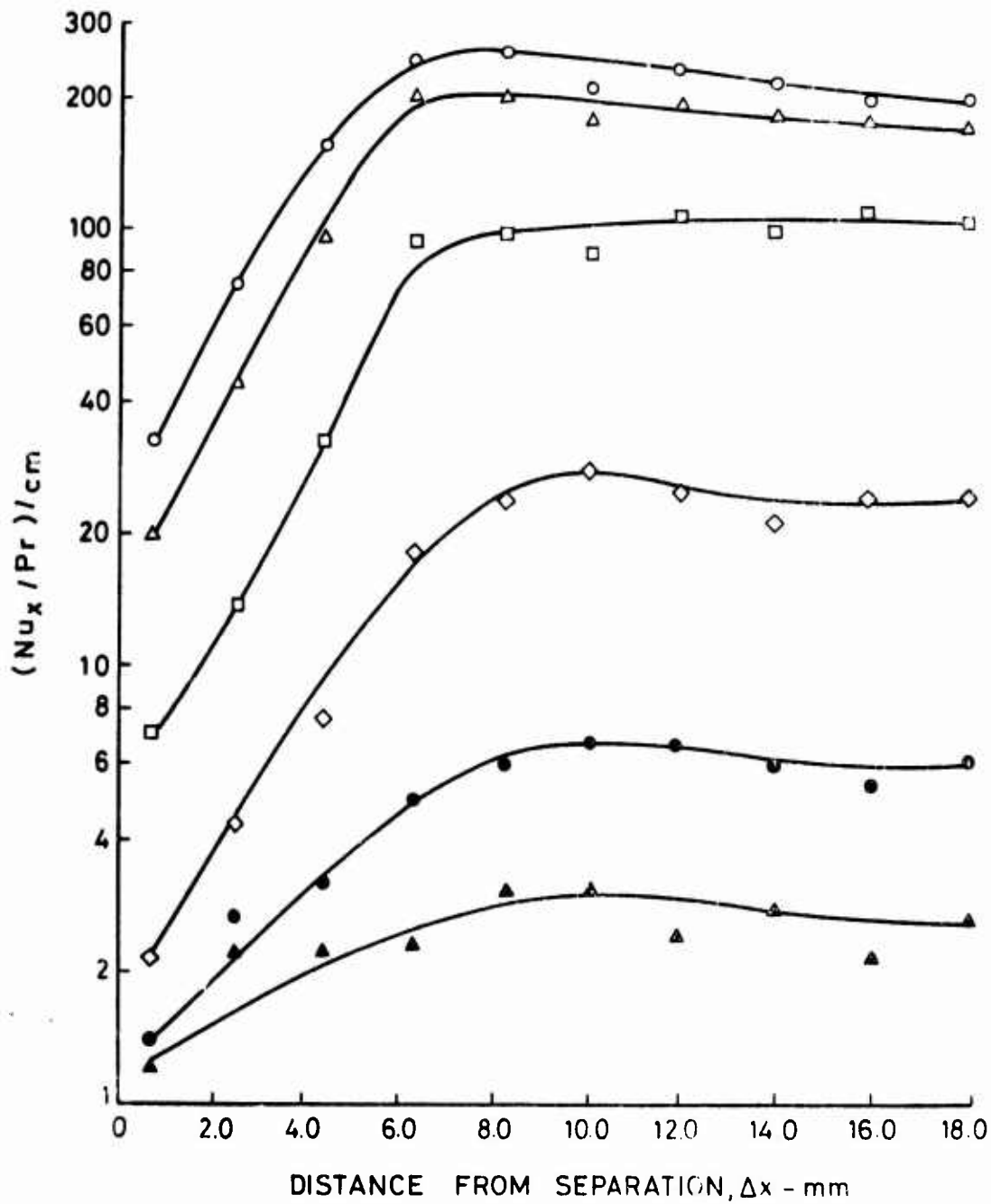


FIGURE 17 -  $(Nu_x / Pr) / cm$  AS A FUNCTION OF  $\Delta x$  FOR MODEL 2

MODEL 3  
h = 2.90 mm

SYMBOL	Re/cm	$\frac{h}{L} Re_L^{1/2}$	Re <sub>L</sub>	M <sub>s</sub>	M <sub>f</sub>
▲	2.5 × 10 <sup>3</sup>	9.1	6.38 × 10 <sup>3</sup>	—	5.5
●	4.0 × 10 <sup>3</sup>	11.5	1.02 × 10 <sup>4</sup>	—	5.5
◇	1.0 × 10 <sup>4</sup>	18.2	2.55 × 10 <sup>4</sup>	8.60	2.37
□	4.0 × 10 <sup>4</sup>	36.3	1.02 × 10 <sup>5</sup>	6.55	2.02
△	1.0 × 10 <sup>5</sup>	57.4	2.55 × 10 <sup>5</sup>	5.20	1.85
○	1.5 × 10 <sup>5</sup>	70.4	3.83 × 10 <sup>5</sup>	4.60	1.77

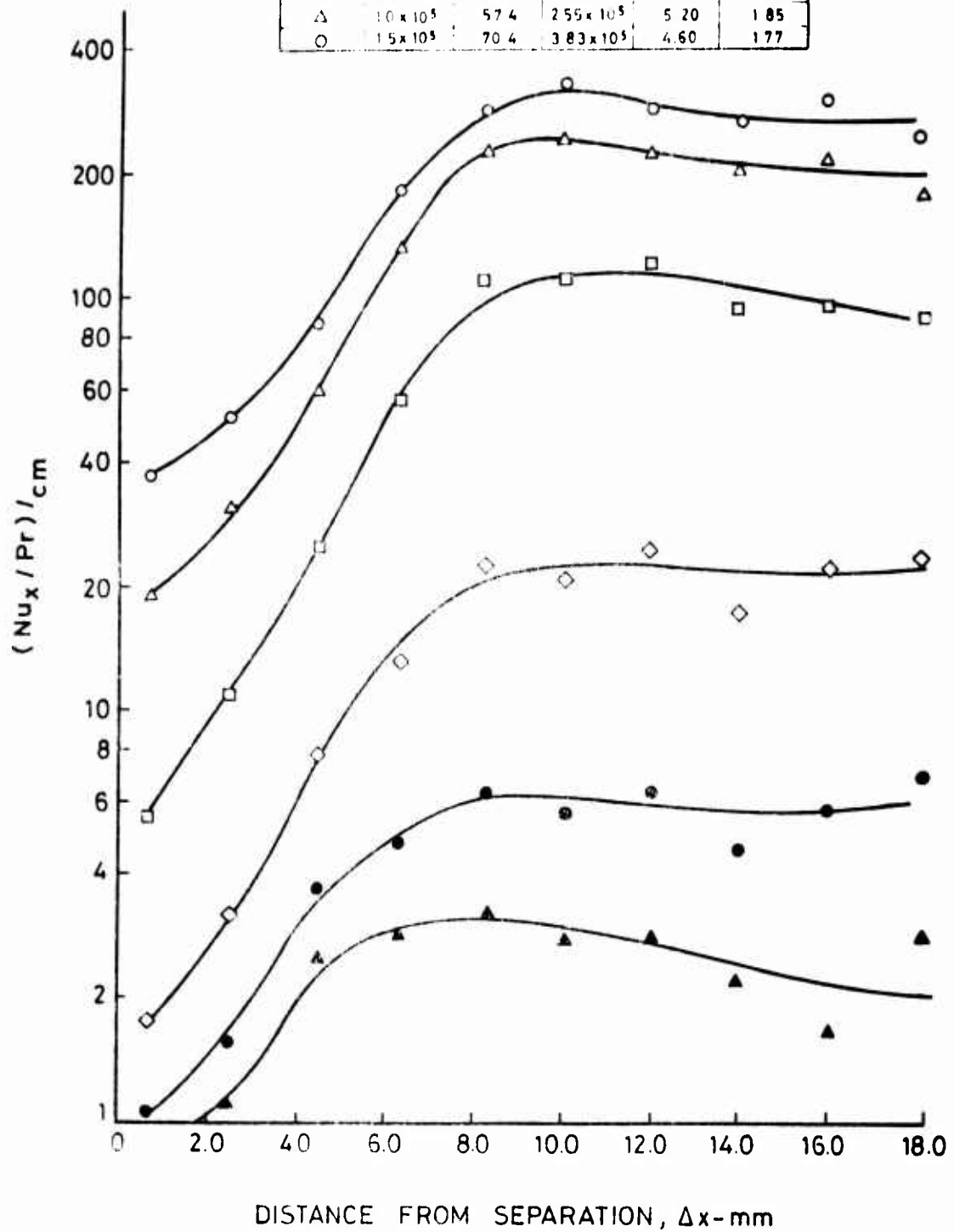
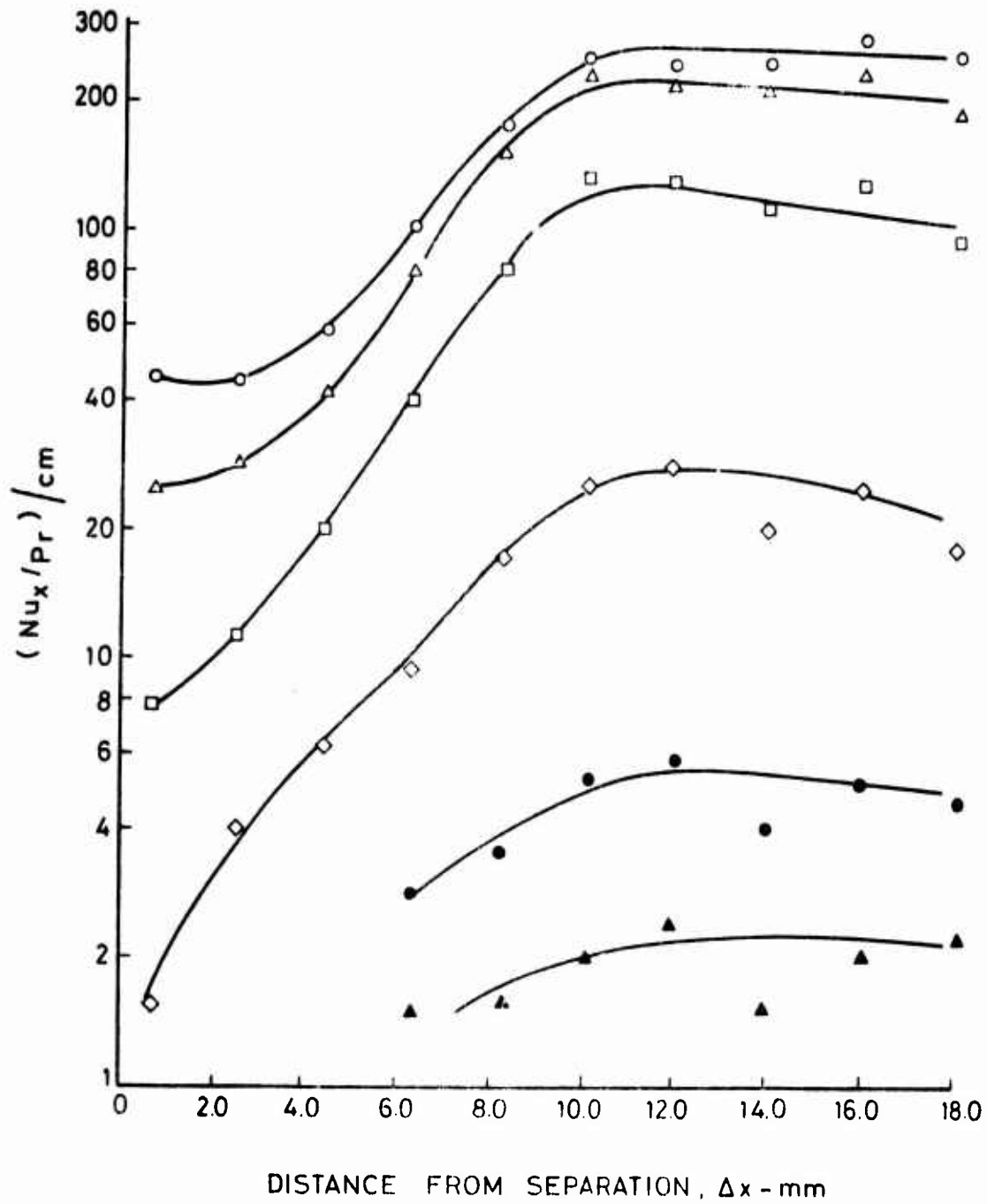


FIGURE 18.  $(Nu_x / Pr) / cm$  AS A FUNCTION OF  $\Delta x$  FOR MODEL 3.

## MODEL 4

 $h = 4.00 \text{ mm}$ 

SYMBOL	$Re_{\infty}$	$Re_L$	$\frac{h}{L} Re_L^{1/2}$	$Ms$	$M_f$
▲	$2.5 \times 10^3$	$6.90 \times 10^3$	12.0	---	5.5
●	$4.0 \times 10^3$	$1.10 \times 10^4$	15.2	---	5.5
◇	$1.0 \times 10^4$	$2.76 \times 10^4$	24.1	8.60	2.37
□	$4.0 \times 10^4$	$1.10 \times 10^5$	48.1	6.55	2.02
△	$1.0 \times 10^5$	$2.76 \times 10^5$	76.1	5.20	1.85
○	$1.5 \times 10^5$	$4.14 \times 10^5$	93.3	4.60	1.77

FIGURE 19 -  $(Nu_x / Pr) / \text{cm}$  AS A FUNCTION OF  $\Delta x$  FOR MODEL 4

SYMBOL	$Re/m$	$Re_L$	$\frac{h}{L} Re_L^{1/2}$	$M_0$	$M_1$
▲	$2.5 \times 10^3$	$9.13 \times 10^3$	2.2	—	5.5
●	$4.0 \times 10^3$	$1.46 \times 10^4$	2.8	—	5.5
◇	$1.0 \times 10^4$	$3.65 \times 10^4$	4.4	8.60	2.37
□	$4.0 \times 10^4$	$1.46 \times 10^5$	8.9	6.55	2.02
△	$1.0 \times 10^5$	$3.65 \times 10^5$	14.1	5.20	1.85
○	$1.5 \times 10^5$	$5.48 \times 10^5$	17.2	4.60	1.77

# MODEL 5

$h = 0.85 \text{ mm}$

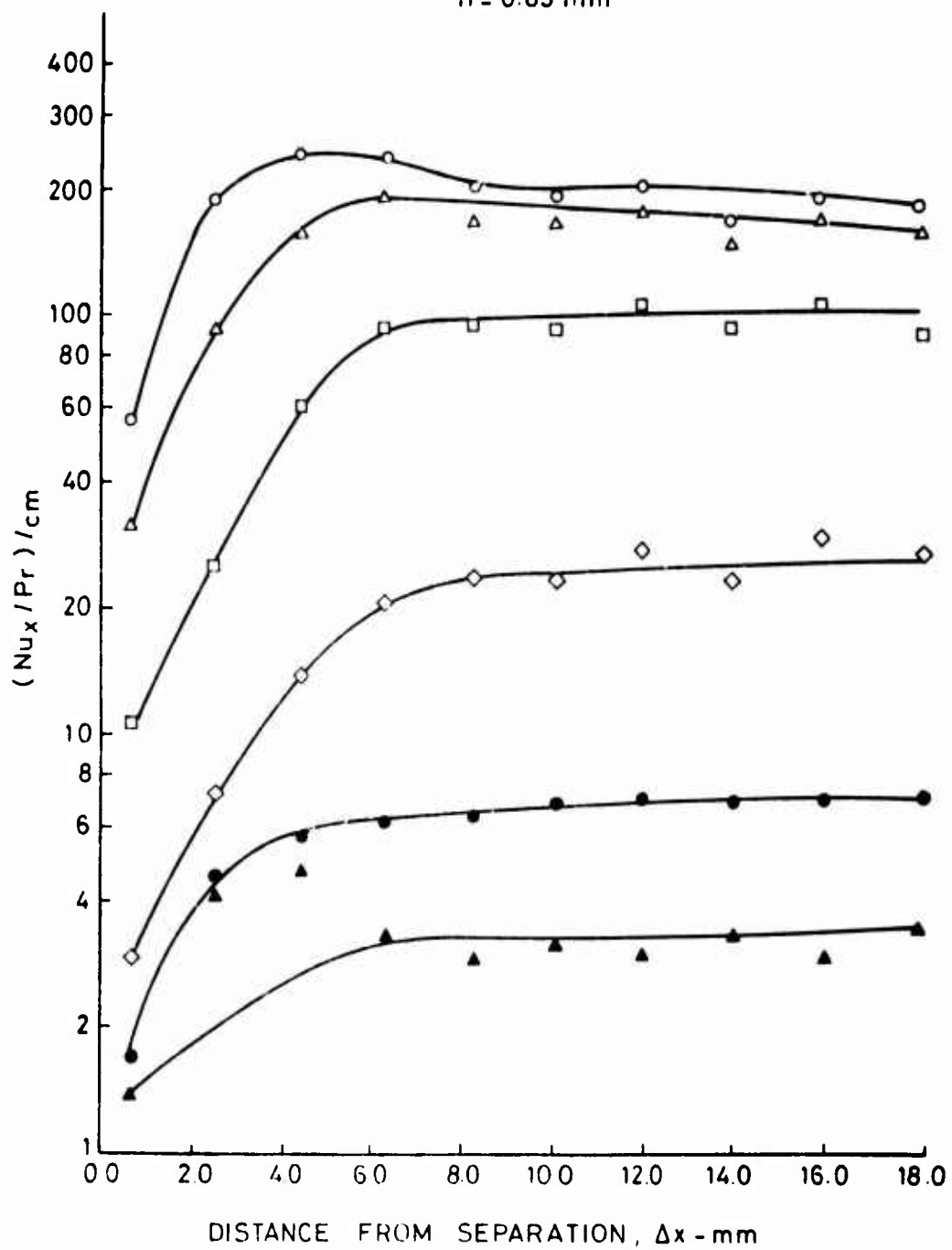


FIGURE 5. VARIATION OF  $Nu_x$  FOR MODEL 5

MODEL 6  
 $h = 190 \text{ mm}$

SYMBOL	$Re/cm$	$Re_L$	$\frac{h}{L} Re_L^{1/2}$	$M_s$	$M_f$
▲	$2.5 \times 10^3$	$9.64 \times 10^3$	4.8	—	5.5
●	$4.0 \times 10^3$	$1.54 \times 10^4$	6.1	—	5.5
◇	$1.0 \times 10^4$	$3.86 \times 10^4$	9.7	8.60	2.37
□	$4.0 \times 10^4$	$1.54 \times 10^5$	19.3	5.55	2.02
△	$1.0 \times 10^5$	$3.86 \times 10^5$	30.6	5.20	1.85
○	$1.5 \times 10^5$	$5.78 \times 10^5$	37.5	4.60	1.77

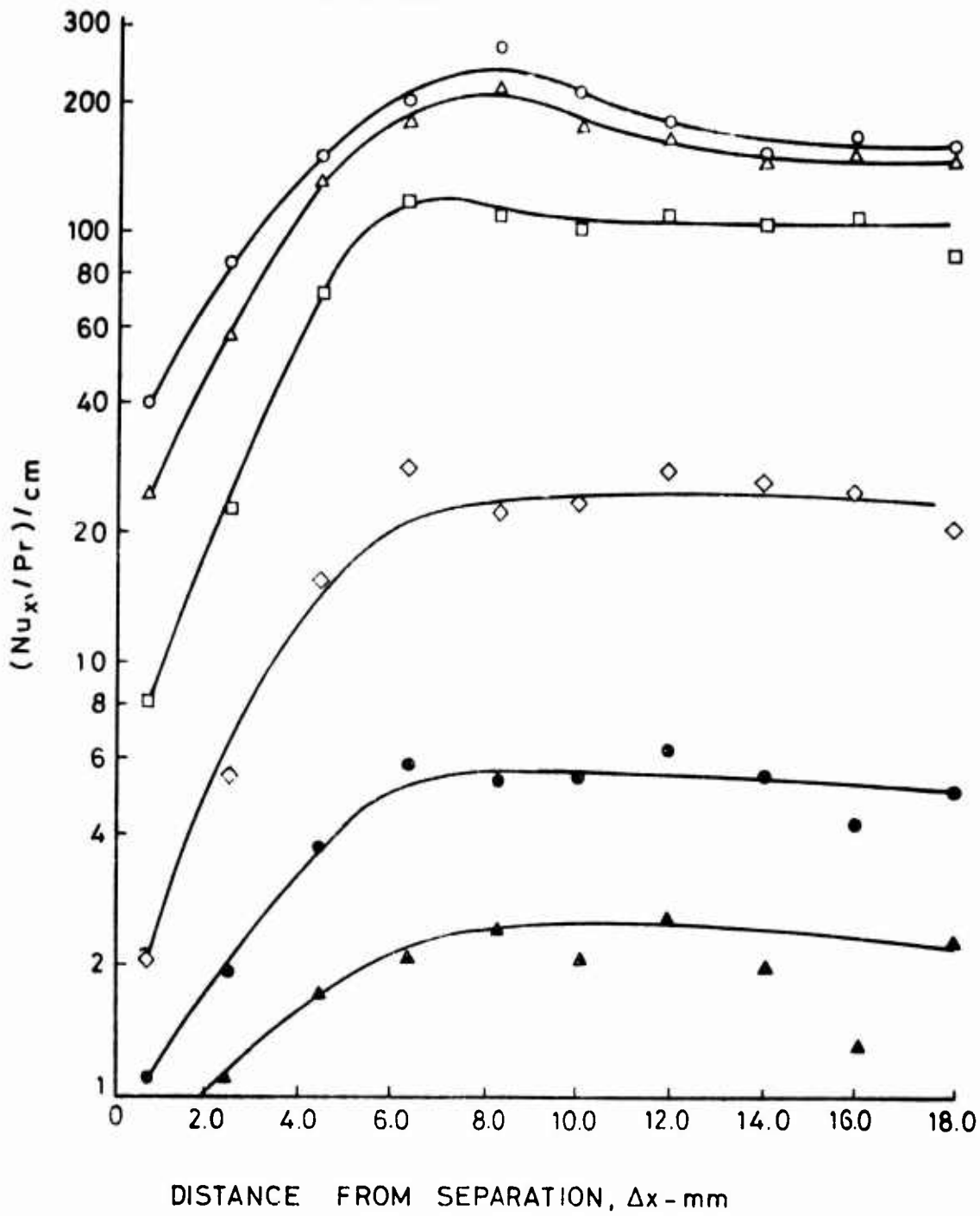


FIGURE 21 -  $(Nu_x/Pr)/cm$  VS. A FUNCTION OF  $\Delta x$  FOR MODEL 6

MODEL 7  
h = 2.90 mm

SYMBOL	$Re_{cm}$	$Re_L$	$\frac{h}{L} Re_L^{1/2}$	$M_S$	$M_f$
▲	$2.5 \times 10^3$	$1.0 \times 10^4$	7.2	—	5.5
●	$4.0 \times 10^3$	$1.62 \times 10^4$	9.1	—	5.5
◇	$1.0 \times 10^4$	$4.05 \times 10^4$	14.4	8.60	2.37
□	$4.0 \times 10^4$	$1.62 \times 10^5$	28.8	6.55	2.02
△	$1.0 \times 10^5$	$4.05 \times 10^5$	45.6	5.20	1.85
○	$1.5 \times 10^5$	$6.08 \times 10^5$	55.8	4.60	1.77

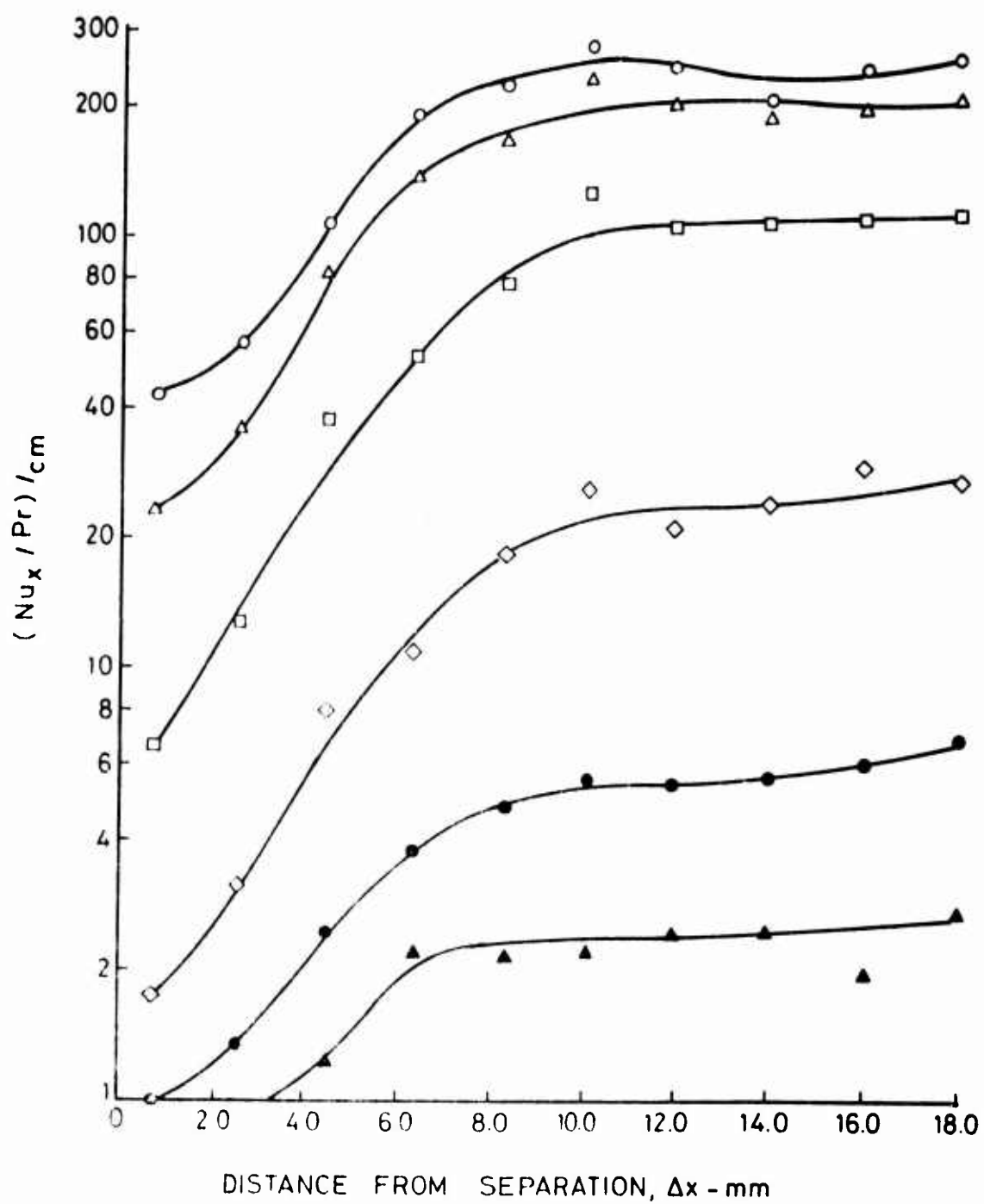


FIGURE 1. Nusselt number as a function of  $\Delta x$  for Model 7.

MODEL 8  
 $h = 4.00 \text{ mm}$

SYMBOL	$Re / \text{cm}$	$Re_L$	$\frac{h}{L} Re_L^{1/2}$	$Ms$	$M_f$
▲	$2.5 \times 10^3$	$1.07 \times 10^4$	9.7	—	5.5
●	$4.0 \times 10^3$	$1.70 \times 10^4$	12.2	—	5.5
◇	$1.0 \times 10^4$	$4.26 \times 10^4$	19.4	8.60	2.37
□	$4.0 \times 10^4$	$1.70 \times 10^5$	58.7	6.55	2.02
△	$1.0 \times 10^5$	$4.26 \times 10^5$	61.3	5.20	1.85
○	$1.5 \times 10^5$	$6.39 \times 10^5$	75.0	4.60	1.77

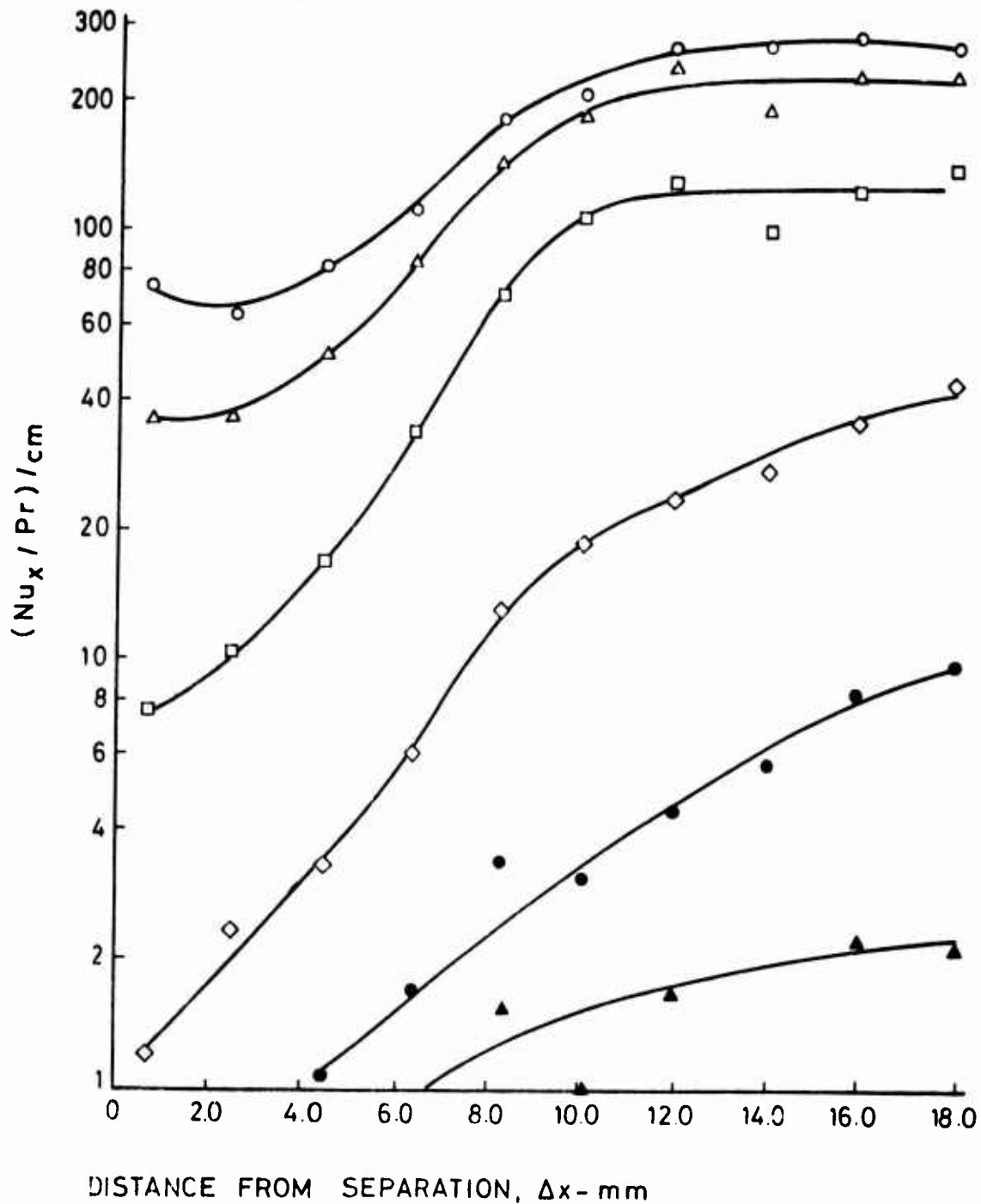


FIGURE 1  $(Nu_x / Pr) / \text{cm}$  AS A FUNCTION OF  $\Delta x$  FOR MODEL 8

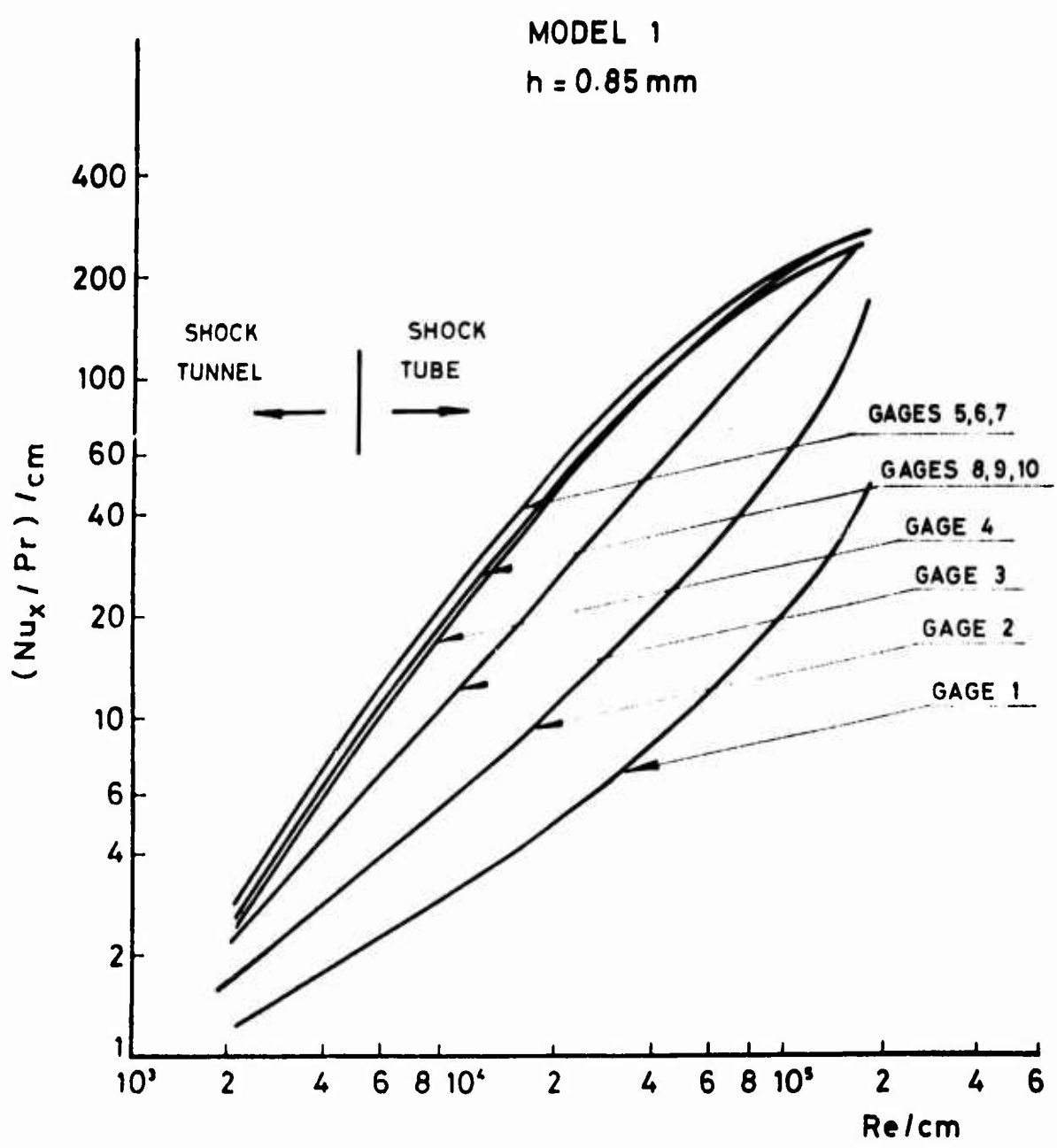


FIGURE 24 -  $(Nu_x / Pr) / \text{cm}$  AS A FUNCTION OF  $Re / \text{cm}$  for Model 1

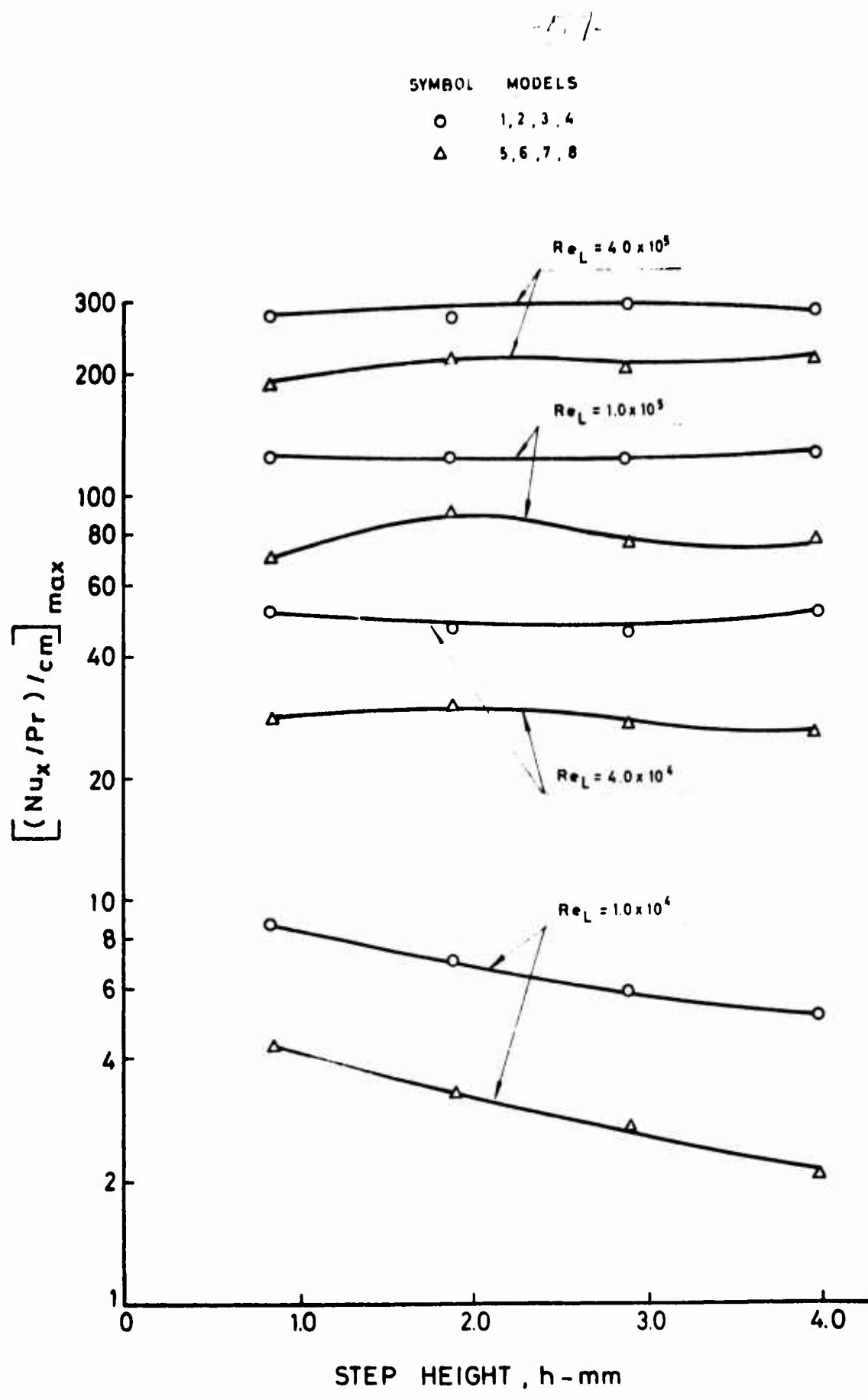


FIGURE 25 -  $[(Nu_x/Pr)/cm]_{max}$  AS A FUNCTION OF  $h$ .

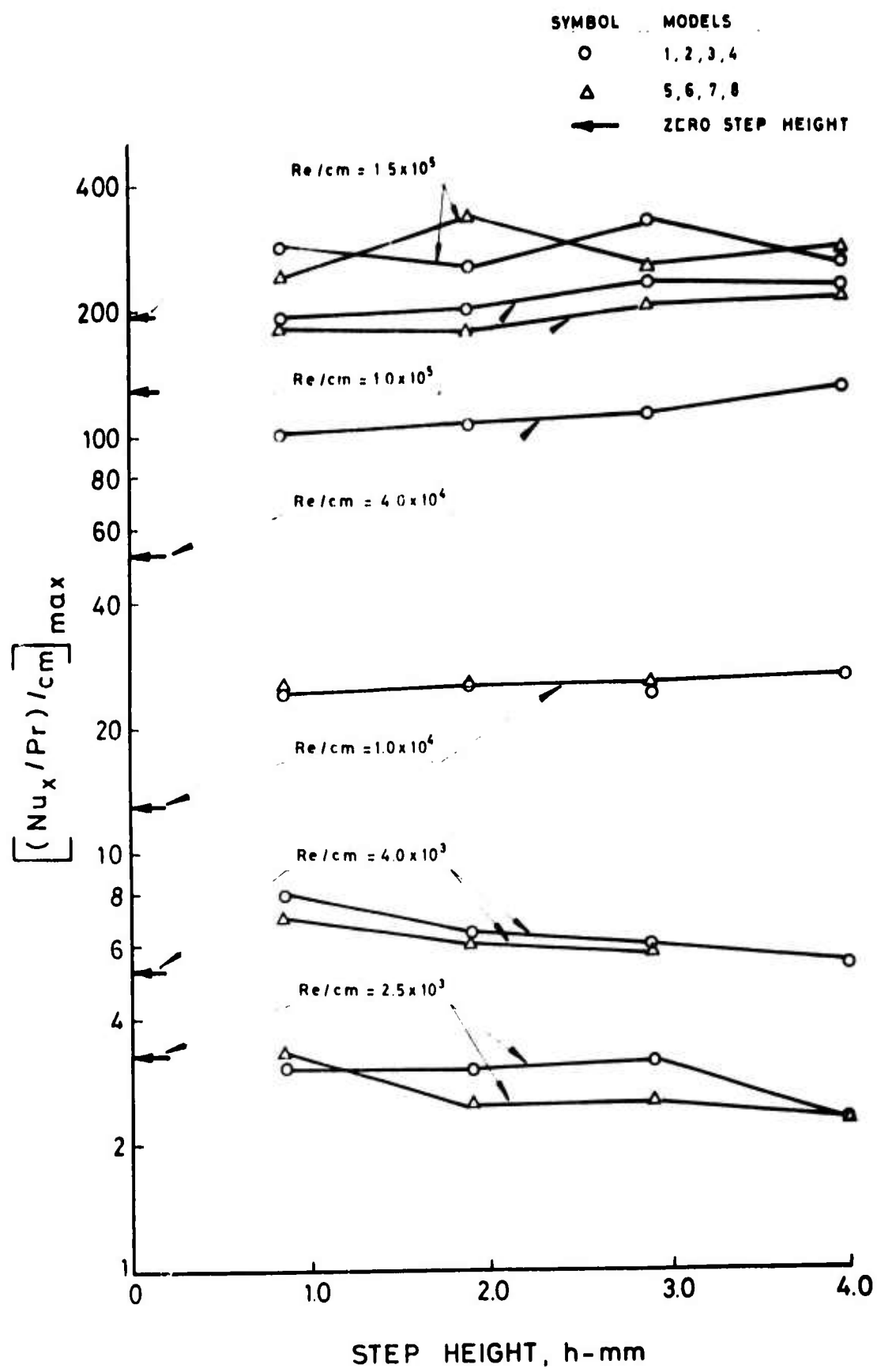


FIGURE 26  $[(Nu_x / Pr) / cm]_{max}$  AS A FUNCTION OF h.

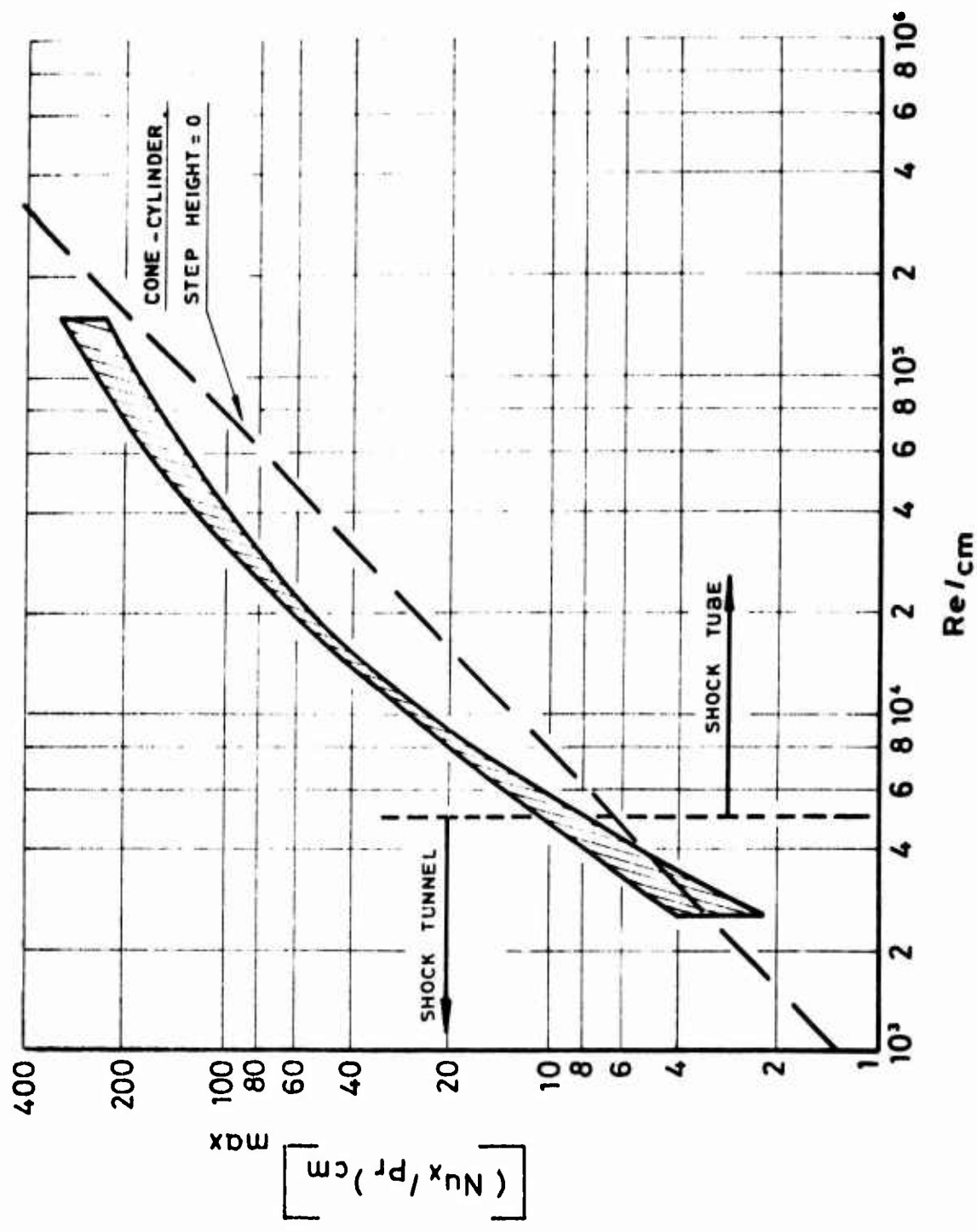


FIGURE 27 -  $[Nu_x/Pr]_{cm}^{max}$  AS A FUNCTION OF  $Re/cm$

-66-

MODEL 1  
 $h = 0.85 \text{ mm}$

SYMBOL	$Re/cm$	$Re_L$
$\diamond$	$2.5 \times 10^3$	$5.38 \times 10^3$
$\circ$	$1.0 \times 10^4$	$2.15 \times 10^4$
$\triangle$	$4 \times 10^4$	$8.60 \times 10^4$
$\square$	$1.0 \times 10^5$	$2.15 \times 10^5$

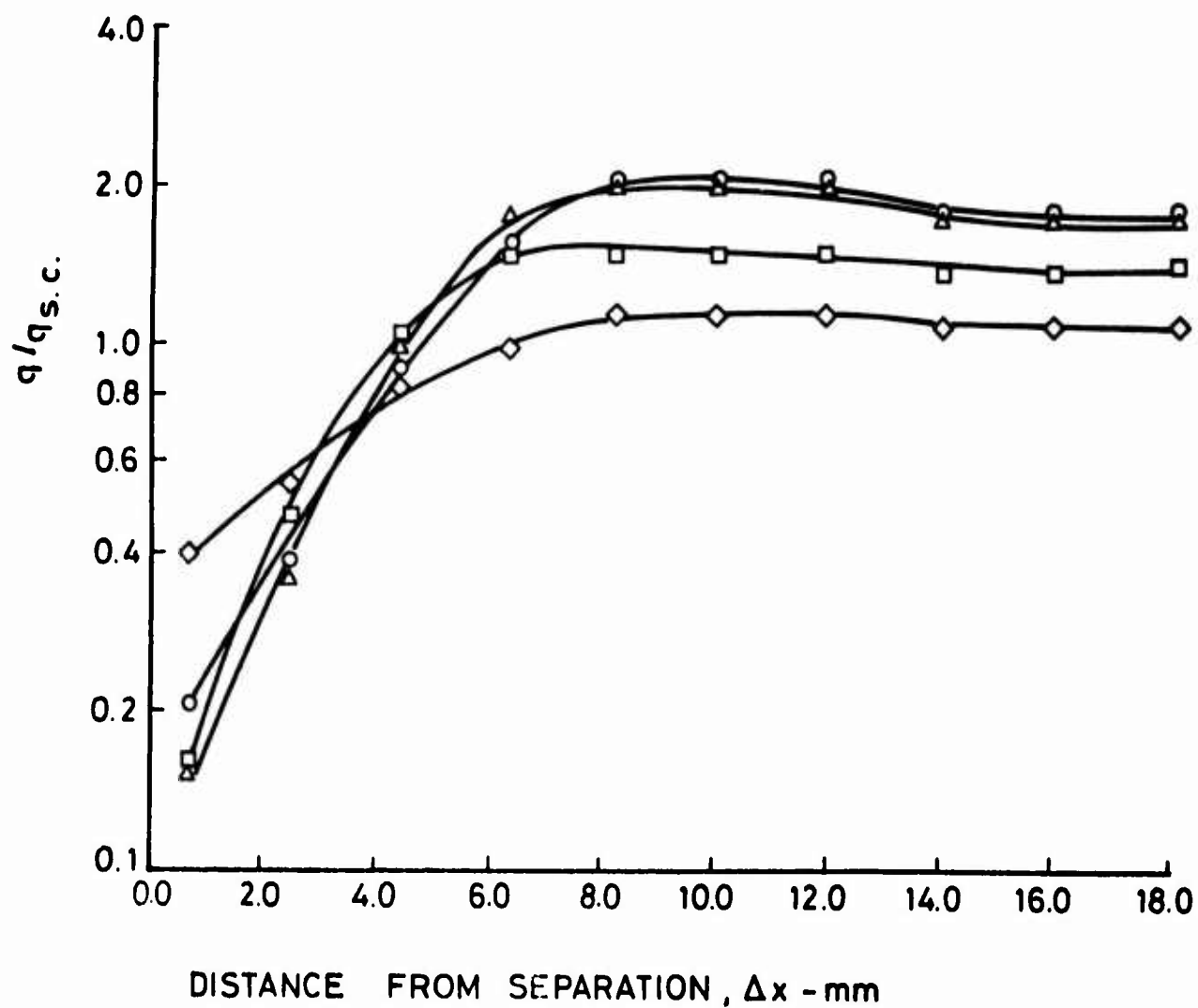


FIGURE 28 -  $q/q_{s,c}$  AS A FUNCTION OF  $\Delta x$  FOR MODEL 1

- 6.1 -

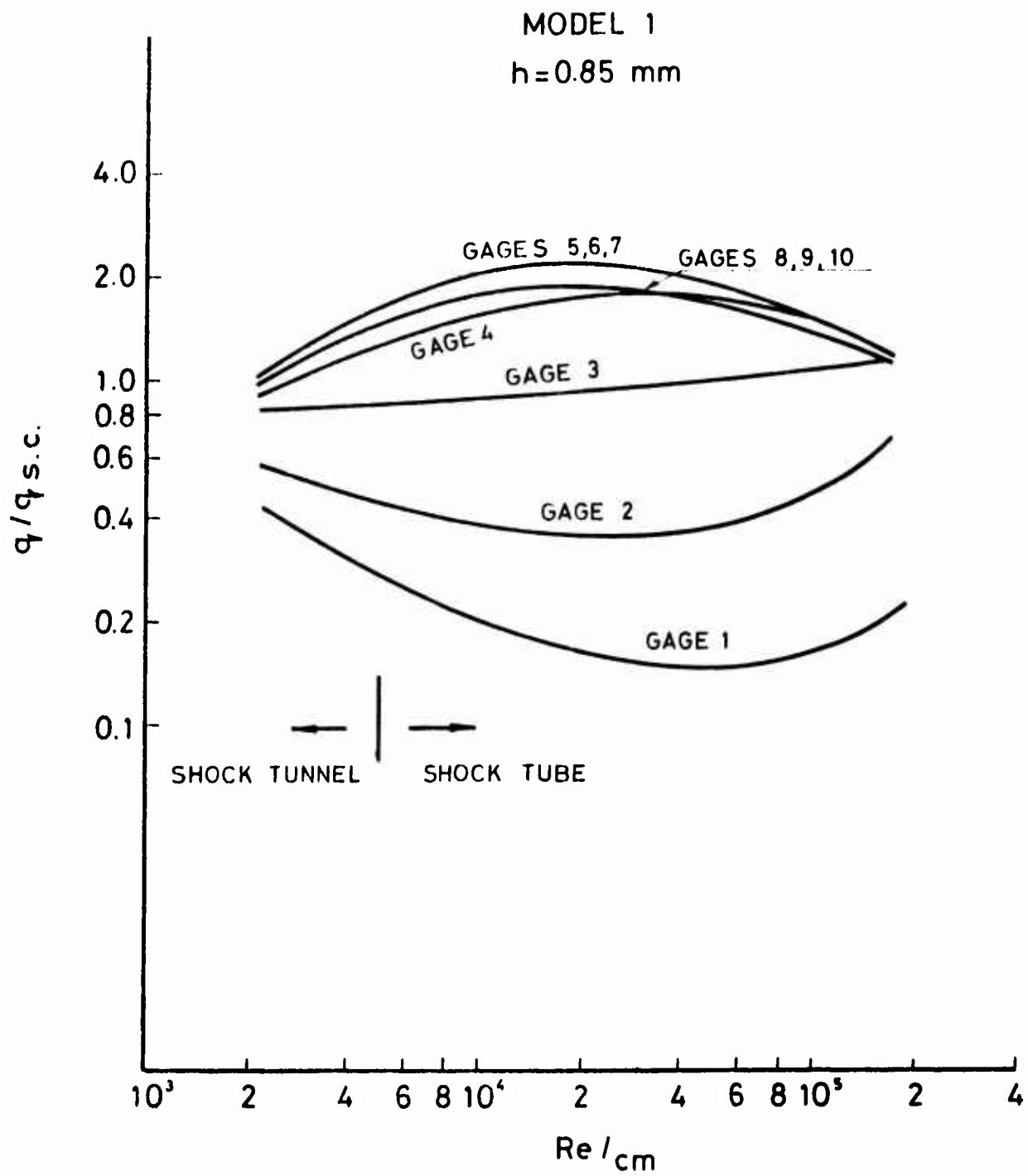


FIGURE 29 -  $q/q_{s.c.}$  AS A FUNCTION OF  $Re/cm$  FOR MODEL 1

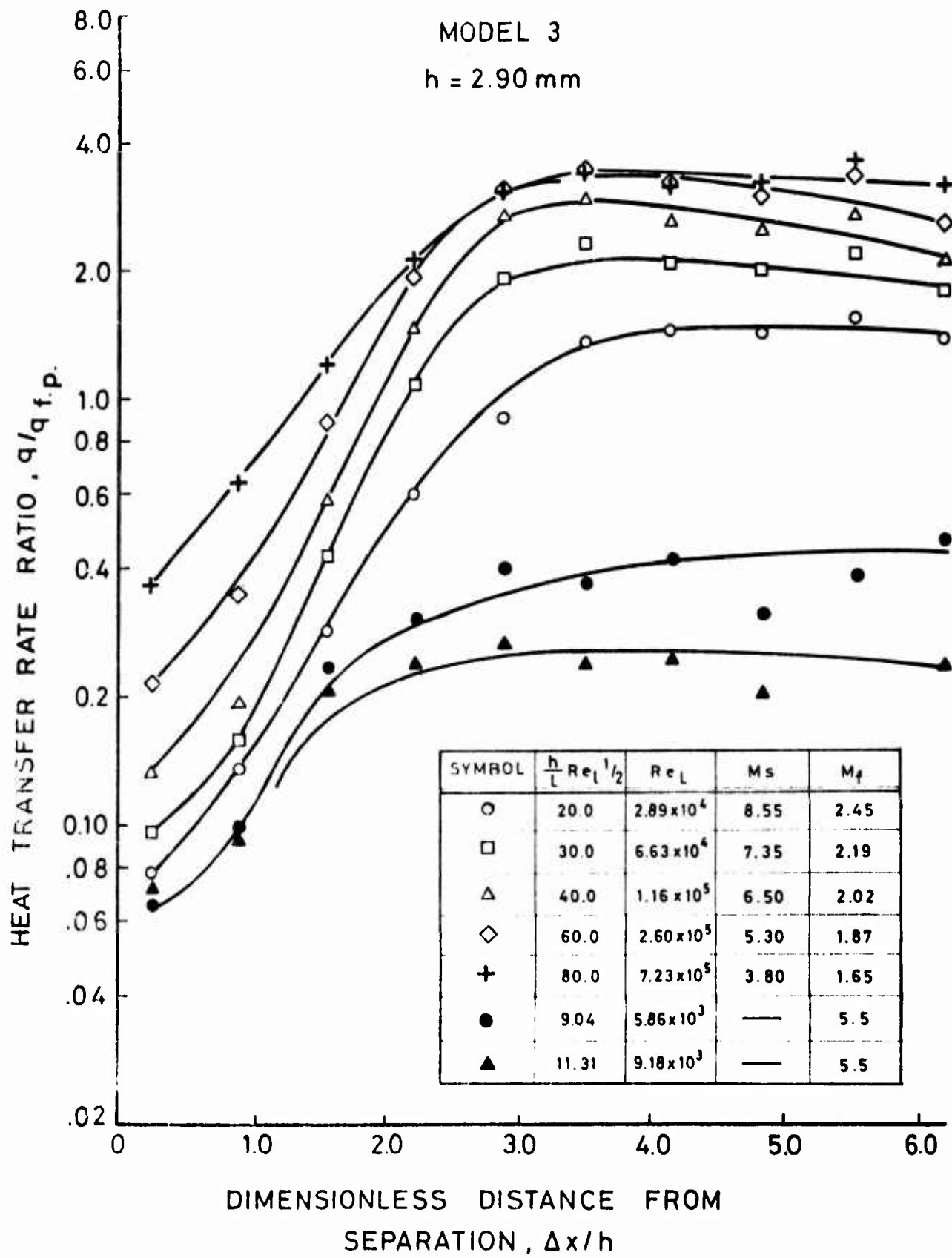


FIGURE 30 -  $q/q_{f,p}$  AS A FUNCTION OF  $\Delta x/h$  FOR MODEL 3

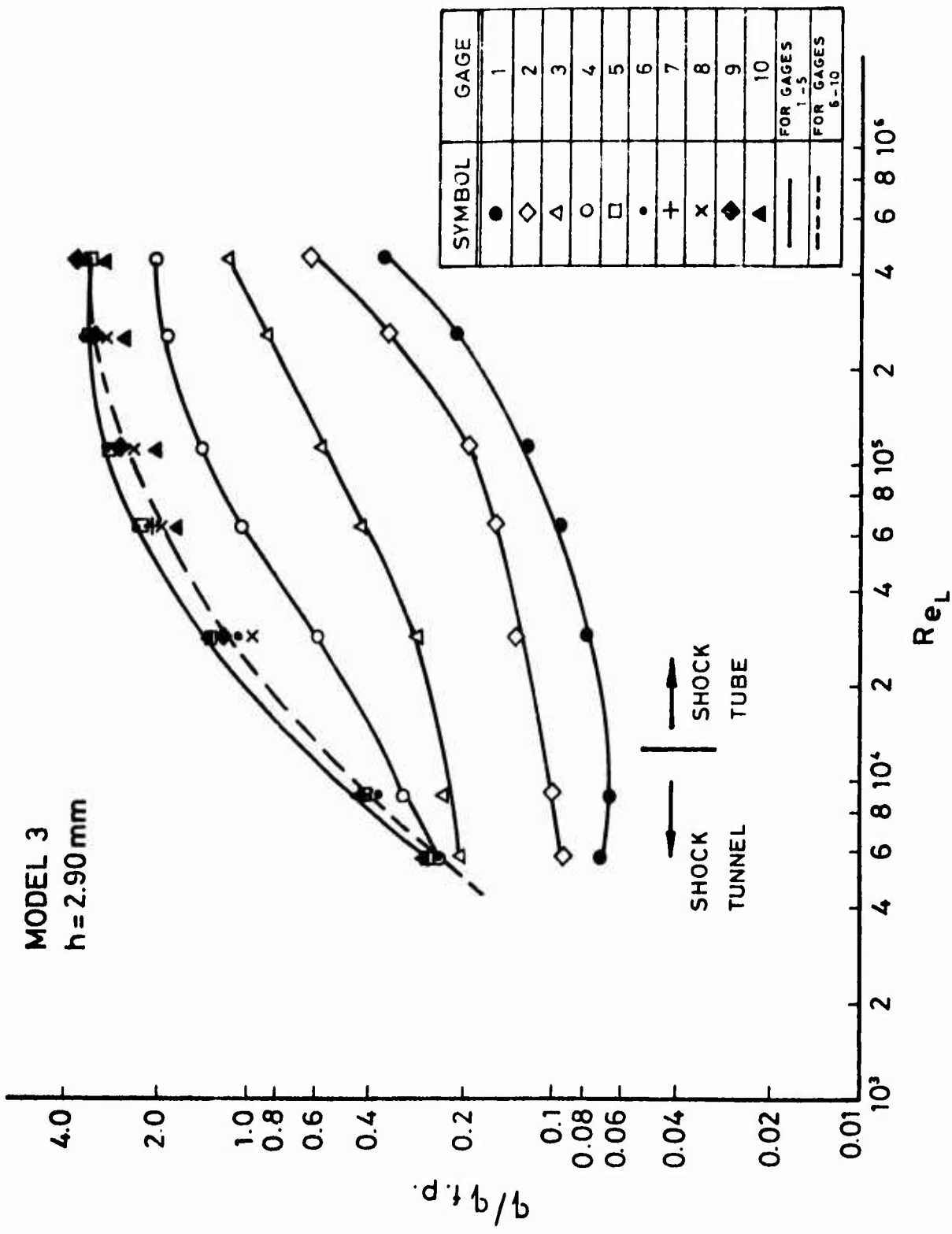


FIGURE 31 -  $q/q_{f.p.}$  AS A FUNCTION OF  $Re_L$  FOR MODEL 3

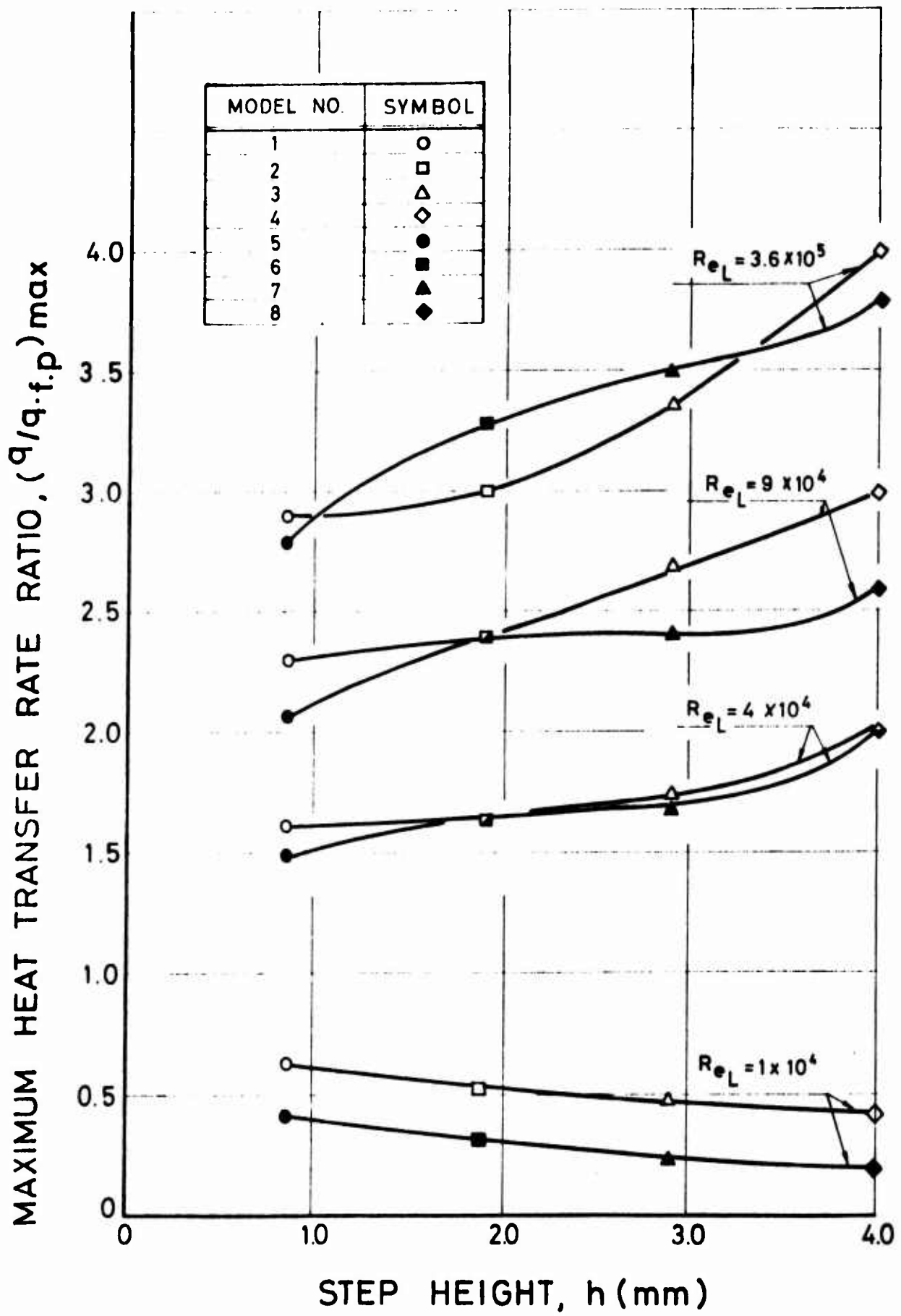


FIGURE 32 -  $(q/q_{f.p.})_{\max}$  AS A FUNCTION OF  $h$

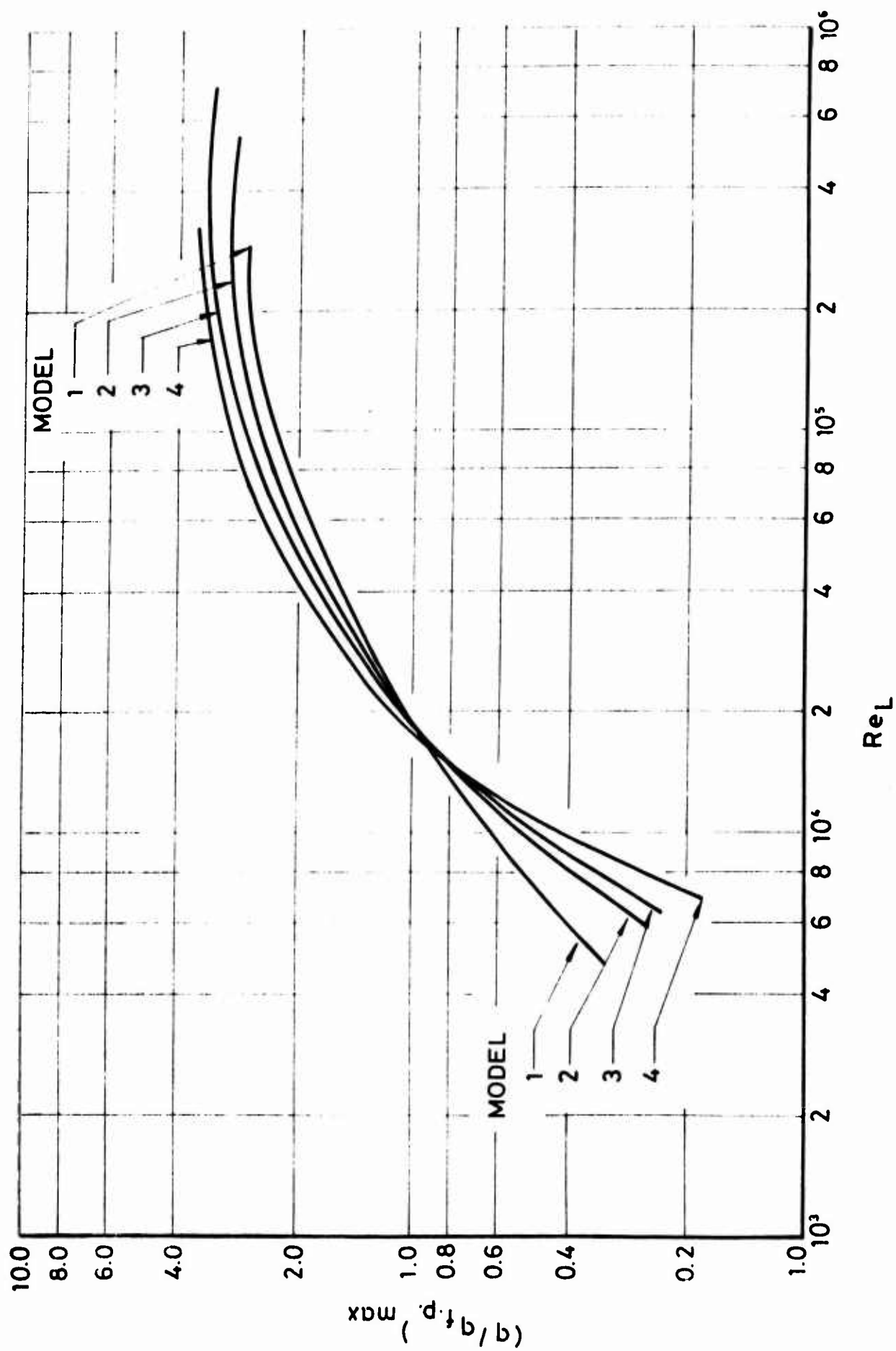


FIGURE 33 -  $(q/q_{f.p.})_{max}$  AS A FUNCTION OF  $Re_L$

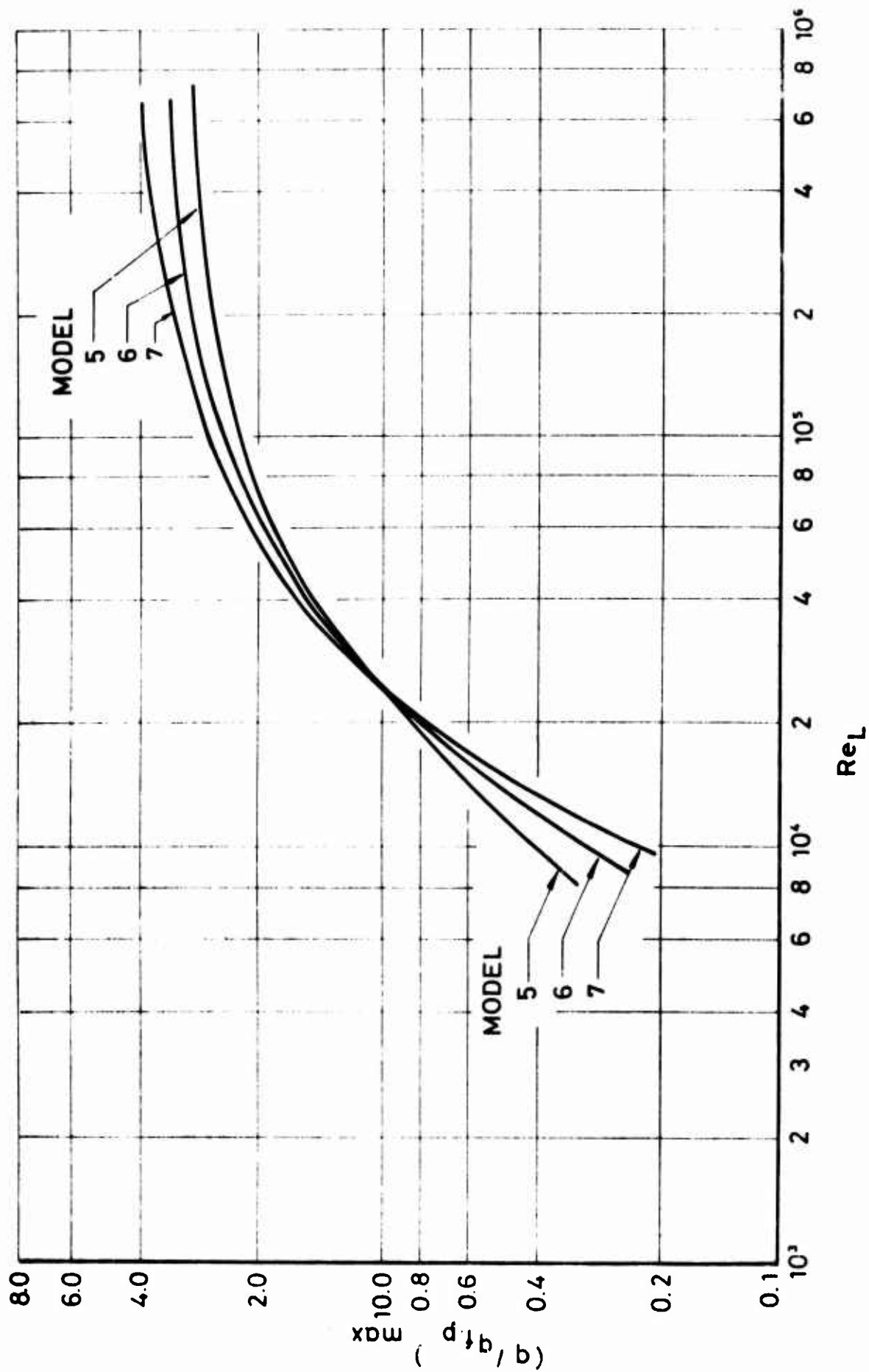


FIGURE 33 (CONTINUED) -  $(q/q_{f.p.})_{\max}$  AS A FUNCTION OF  $Re_L$

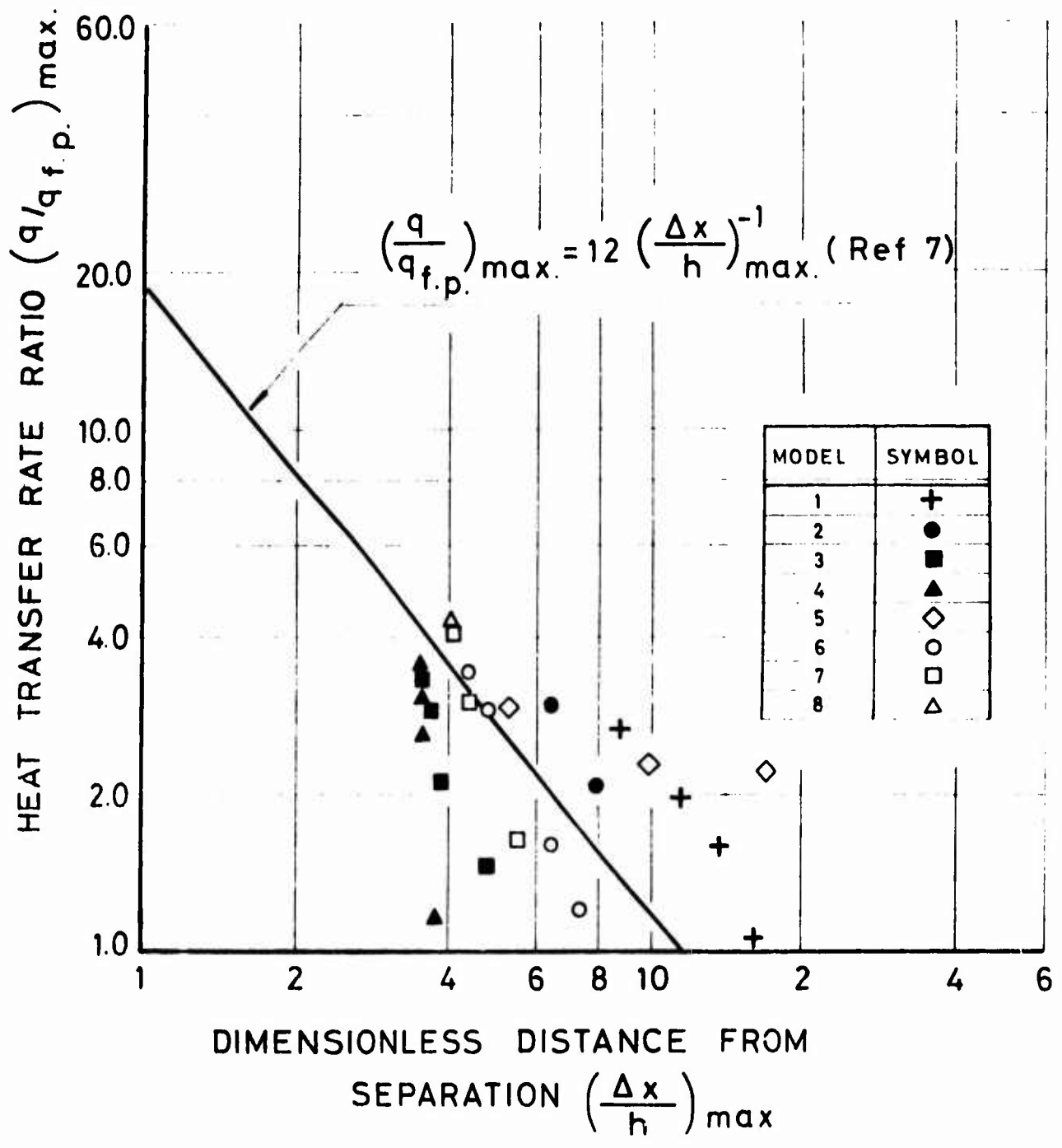


FIGURE 51 - MAXIMUM HEAT TRANSFER RATE AT REATTACHMENT AS A FUNCTION OF  $(\Delta x/h)_{max}$

MODEL 11  
 $h = 10.2 \text{ mm}$

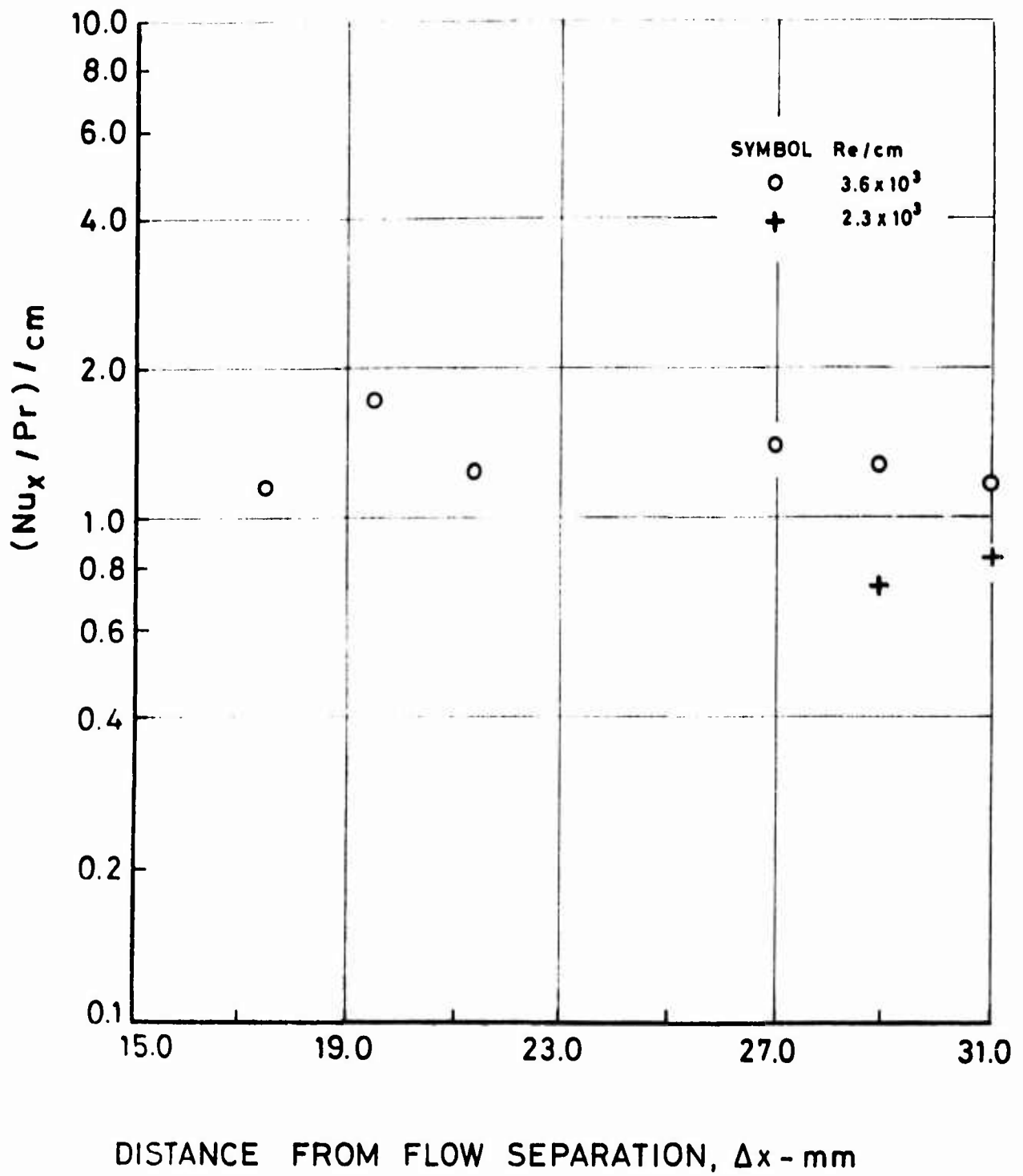


FIGURE 35 -  $(Nu_x / Pr) / \text{cm}$  AS A FUNCTION OF  $\Delta x$  FOR MODEL 11